
A GENERALISED LINEAR MODEL FRAMEWORK FOR VARIATIONAL AUTOENCODERS BASED ON EXPONENTIAL DISPERSION FAMILIES

TECHNICAL REPORT

Robert Sicks^{*1} Ralf Korn^{1,2} Stefanie Schwaar¹

¹Department of Financial Mathematics, Fraunhofer ITWM, Kaiserslautern, Germany

²Department of Financial Mathematics, TU Kaiserslautern, Kaiserslautern, Germany

June 6, 2022

ABSTRACT

Although variational autoencoders (VAE) are successfully used to obtain meaningful low-dimensional representations for high-dimensional data, aspects of their loss function are not yet fully understood. We introduce a theoretical framework that is based on a connection between VAE and generalized linear models (GLM). The equality between the activation function of a VAE and the inverse of the link function of a GLM enables us to provide a systematic generalization of the loss analysis for VAE based on the assumption that the distribution of the decoder belongs to an exponential dispersion family (EDF). As a further result, we can initialize VAE nets by maximum likelihood estimates (MLE) that enhance the training performance on both synthetic and real world data sets.

1 Introduction

Variational autoencoders (VAE) are described by Goodfellow et al. (2016) as an “excellent manifold learning algorithm” due to the fact that the model is forced “to learn a predictable coordinate system that the encoder can capture”. VAE do so by using a regularization term in order to get to low energy regions. According to LeCun (2020), regularization like in the VAE case helps to keep the energy function smooth, which is desirable for the model in order to learn meaningful dependencies (e.g. to fill blanks). In contrast, maximum likelihood approaches push down the energy surface only at training sample regions. Therefore, their inherent objective is “to make the data manifold an infinitely deep and infinitely narrow canyon” (see LeCun 2020).

Learning meaningful dependencies is a desirable concept for advancing deep learning. Hence, there exists an interest in understanding and developing VAE. Recent work aims on explaining and overcoming well-known pitfalls of VAE, such as spurious global optima (see Dai and Wipf 2019), posterior collapse (see Lucas et al. 2019 and van den Oord et al. 2017) or prior posterior mismatch (see Dai and Wipf 2019 and Ghosh et al. 2020). In these works, a specific decoder distribution is assumed to analyse the loss surface of the model or to look at the training behaviour.

In this work, we answer the following research question:

Is there a way to generalize the loss analysis of VAE based on the decoder distribution?

For this, we establish a connection between VAE and generalized linear models (GLM) and provide a framework for analysing VAE based on the decoder distribution. By doing so, we generalize works of Dai et al. (2018), Lucas et al. (2019) and Sicks et al. (2020). We provide an approximation to the evidence lower bound (ELBO), which is exact in the Gaussian distribution case (see also Dai et al. 2018 and Lucas et al. 2019) and a lower bound for the Bernoulli distribution case (see also Sicks et al. 2020). Further, we analyse the maximum likelihood estimators (MLE) of this

^{*}Corresponding author

approximation and find that the choice of decoder activation function does not affect the maximum. Using the MLE as initialization, we also show that the training performance of a VAE net can be enhanced.

As GLM are based on exponential dispersion families (EDF), the analysis is based on the distribution assumption for the decoder model. This is favourable as VAE are applied in various different fields (with different distribution assumptions), as e.g.: anomaly detection using Gaussian distribution (see Xu et al. 2018), molecules representation using Bernoulli distribution (see Blaschke et al. 2018), image compression using Bernoulli distribution (see Duan et al. 2019) or multivariate spatial point processes using Poisson distribution (see Yuan et al. 2020).

This work is structured as follows: In Section 2, we give a motivation as well as an overview of related work. In Section 3, we present the theoretical background and our results that are a consequence of connecting VAE and GLM. Afterwards in Section 4, we provide simulations validating our theoretical results and show that these can be used for deep VAE. In Section 5, we summarize our contributions and point out future research directions.

2 Motivation and Related Work

Throughout our theoretical analysis, we consider VAE with arbitrary encoder and one-layer decoder. Our main contribution is to interpret this one-layered decoder as a GLM (see Section 3.2). This perspective allows us to identify well-known activation functions as the reciprocal of link functions of GLM. Therefore, we are able to provide a systematic generalization of the loss analysis for VAE based on the assumption that the distribution of the decoder belongs to an EDF.

Even though the decoder architecture is arguably simple, analysing the critical points and the loss landscapes of VAE helps to understand these models better. Using this architecture and approach, Dai et al. (2018) show connections to probabilistic principal component analysis (pPCA), Lucas et al. (2019) analyse posterior collapse and Sicks et al. (2020) bound the ELBO for a Bernoulli VAE from below.

Given an one-layered decoder with Gaussian distribution assumption, the model (more specifically $P_\theta(Z|X)$ ¹) becomes tractable. Lucas et al. (2019) use this for their analysis and show that in this case the ELBO becomes exact, as one has $q_\phi(Z|X) = P_\theta(Z|X)$. Still, the main motivation for VAE is the assumption of intractability (see Kingma and Welling 2014), where the recognition model $q_\phi(Z|X)$ is used to approximate the intractable posterior $P_\theta(Z|X)$. In case of tractability as for the Gaussian model, an established alternative is the EM algorithm.

Under the one-layer decoder assumption, the model does not necessarily become tractable. E.g. for a Bernoulli decoder, the model stays intractable (see Aitchison and Shen 1980).

Our framework can serve as a stepping stone to theory for more rigorous models as it yields

- known results for the “good to handle” Gaussian case. To be more specific, we provide an equivalent optimization target to those in Dai et al. (2018) and Lucas et al. (2019).
- interpretational guidance for intractable settings like the Bernoulli case. Our results for the sigmoid² activation are equivalent to the results in Sicks et al. (2020). Even though the resulting target is only approximative, our simulation in Section 4 for the Bernoulli case shows reasonable results on real data (i.e. frey data).
- the possibility to use GLM tools to further analyse VAE and to extend the analysis to include more EDF distributions (e.g. the Gamma distribution).

In the following, we give an overview of literature for analysing Autoencoders and VAE as well as on GLM used in the context of neural nets.

Bourlard and Kamp (1988) show for autoencoders with linearised activations that the optimal solution is given by the solution of a singular value decomposition (SVD). Baldi and Hornik (1989) extend these results and analyse the squared error loss of autoencoders for all critical points.

Dai et al. (2018) analyse Gaussian VAE with the same architecture as in this work. They show connections to pPCA and robust PCA as well as smoothing effects for local optima of the loss landscape.

Zhou and Liang (2018) provide analytical forms for critical points and characterize the values of the corresponding loss functions as well as properties of the loss landscape for one-hidden layer ReLU autoencoders.

¹The expressions $P_\theta(Z|X)$ and $q_\phi(Z|X)$ are defined as in Kingma and Welling (2014).

²Actually, we mean the logistic function. It has become common to use the term sigmoid function for this special case. Therefore, in the following we keep on using the term sigmoid function.

Dai and Wipf (2019) analyse deep Gaussian VAE. Assuming, the existence of an invertible and differentiable mapping between low-rank manifolds in the sample space and the latent space, they show that spurious global optima exist, which do not reflect the data-generating manifold appropriately.

Kunin et al. (2019) consider regularizations on linear autoencoders and analyse the loss-landscape for different regularizations. They show regularized linear autoencoders are capable of learning the principal directions and have connections to pPCA.

Lucas et al. (2019) extend results of Dai et al. (2018) to analyse the posterior collapse. They do this by analysing the difference from the true marginal to the ELBO which is possible under Gaussian assumptions, as $P_\theta(Z|X)$ becomes tractable. Furthermore, they provide experimental results on the posterior collapse for deep non-linear cases.

Sicks et al. (2020) formulate a lower bound for the ELBO of a Bernoulli VAE with the same architecture as in this work. They use the MLE to derive an initialization scheme and empirically compare it on synthetic data.

Wüthrich (2020) describes connections between GLM and neural network regression models, by interpreting the last layer of a neural net as GLM. With this, he is able to use a L^1 regularized neural net to learn representative features to improve a standard GLM. Furthermore, favourable properties (as for an actuarial context, the "balance property") are achieved with a proposed hybrid model.

3 Theoretical Background and Advancements

For realizations $x^{(1)}, \dots, x^{(N)}$ of a random variable (r.v.) X , we consider a VAE as in Kingma and Welling (2014) with the ELBO \mathcal{L} , given by

$$\mathcal{L}(x^{(i)}; \phi, \theta) := E_{Z \sim q_\phi(\cdot|x^{(i)})} \left[\log P_\theta(x^{(i)}|Z) \right] - D_{KL} \left(q_\phi(Z|x^{(i)}) || P_\theta(Z) \right). \quad (1)$$

Interpreting the expectation in this expression as autoencoder yields the encoder $q_\phi(Z|x^{(i)})$ and the decoder $P_\theta(x^{(i)}|Z)$. We further assume that the encoder produces $\mu_z^{(i)} := f_1(x^{(i)}, \phi)$ and $0 \prec \Sigma_z^{(i)} := S_z^{(i)} S_z^{(i)T}$, with $S_z^{(i)} := f_2(x^{(i)}, \phi)$, where f_1 and f_2 are arbitrary functions including affine transformations. The decoder is one-layered with a not necessarily linear activation function $\mathbf{m}(\cdot)$, weights $W \in \mathbb{R}^{d \times \kappa}$ and biases $b \in \mathbb{R}^d$.

In the following, we first provide the theoretical background on GLM and EDF. Then, we show how the decoder can be interpreted as GLM. Finally, given this new perspective on VAE, we present theoretical results and analyse MLE for the resulting approximation.

3.1 The GLM and EDF

Nelder and Wedderburn (1972) introduce GLM, providing a generalization of linear statistical models and thus of well-known statistical tools, such as analysis of variance (ANOVA), deviance statistics and MLE (see also McCullagh and Nelder 1989). GLM consist of three parts: A random component X with a distribution belonging to the EDF, a systematic component given as affine mapping of features Z used to estimate $\mathbb{E}(X|Z)$, and a link function connecting these two components. Hereby, the EDF is defined by the structure of the density.

Definition 1. *We say the distribution of X given Z belongs to the exponential dispersion family (EDF), if the density can be written as*

$$\log P_{\vartheta, \varphi}(X|Z) = \frac{X \cdot \vartheta(Z) - F(\vartheta(Z))}{\varphi} + K(X, \varphi), \quad (2)$$

where F and K are one-dimensional functions. $F : \mathbb{R} \rightarrow \mathbb{R}$ is also called the log-normalizer. It ensures that integration w.r.t. the density in (2) over the support of X is equal to one. $\vartheta(Z) \in \Theta$ is the location parameter. Θ is an open, convex space with $\Theta = \left\{ \vartheta \in \mathbb{R} : \int_x \exp \left(\frac{x\vartheta}{\varphi} + K(x, \varphi) \right) dx < \infty \right\}$. $\varphi > 0$ is called the dispersion parameter and independent of Z .

The EDF is studied in Barndorff-Nielsen (2014), Jørgensen (1986) and Jørgensen (1987). Several well-known distributions, like the Gaussian, Bernoulli and Poisson distribution, belong to this family (see Table 1 in supplementary material Section A for the respective representations).

Lemma 1. *Let the distribution of a one-dimensional r.v. $X \sim P_{\vartheta, \varphi}(X|Z)$ given Z belong to the EDF. Then, it holds $\mathbb{E}(X|Z) = F'(\vartheta(Z))$ and $\text{Var}(X|Z) = \frac{1}{\varphi} F''(\vartheta(Z))$. Furthermore, the log-partition function F is convex and possesses all derivatives.*

The proof for the unconditional case is performed in Theorem 7.1, Corollary 7.1 and Theorem 8.1 in Barndorff-Nielsen (2014). The statement for the conditional case is found analogously.

3.2 The decoder as GLM

We interpret the decoder $P_\theta(x^{(i)}|Z)$ as GLM. Therefore, we assume that the independent identical marginal distributions of X given Z belong to an EDF, where they share the same φ . With a realization $z \sim q_\phi(\cdot|x^{(i)})$ from the encoder, the parameters of the decoder $P_\theta(x^{(i)}|z)$ are given by $\theta = \{\vartheta, \varphi\}$, with $\vartheta = (\vartheta_1(z), \dots, \vartheta_d(z))$.

Part of the training objective of a VAE implementation is to construct outputs that resemble the inputs to a high degree. Therefore, the decoder reports the value

$$z \mapsto \mathbb{E}_{\vartheta, \varphi} (x^{(i)}|Z = z),$$

the (conditional) expectation given a latent representation created by the encoder. Training on the decoder is conducted by updating the parameters in the set θ . In consensus with GLM (see McCullagh and Nelder 1989), we define the linear predictor $\eta = W \cdot z + b$, with $W \in \mathbb{R}^{d \times \kappa}$ and $b \in \mathbb{R}^d$. Given an activation function m , we set³

$$m(\eta) = \mathbb{E}_{\vartheta, \varphi} (X|z)$$

and according to Lemma 1, we have

$$\mathbb{E}_{\vartheta, \varphi} (X|z) = F'(\vartheta).$$

With the linear predictor introduced, we have for our decoder parameter set $\theta = \{W, b, \varphi\}$.

Obviously, $m = F'$ is a special choice for which we have $\eta = \vartheta$. We call this choice of m the “canonical activation”. This name originates from the “canonical link function”. As mentioned in Section 3.1, for GLM we define a link function g connecting the systematic component of the model η to the random component $\mathbb{E}_\theta (X|z)$. This function is called canonical if $g = (F')^{-1}$. Hence, the canonical activation is the inverse of the canonical link.

A canonical function has the advantage of an affine mapping from the net parameters to the EDF parameters. This will simplify the derivation of our theoretical results below. Apart from canonical activations, we want to provide theory for a more general case. We consider any activation that scales the systematic component η to ϑ , s.t. for $\beta \in \mathbb{R} \setminus \{0\}$ we have

$$\vartheta = \beta \cdot \eta. \tag{3}$$

We call activations applying to this “linearly canonical activation”. Obviously, for canonical activations we have $\beta = 1$.

Though this theory is not new, we want to stress the point that commonly used activation functions in machine learning are linearly canonical activations. Two examples in Section A of the supplementary material illustrate this for the sigmoid and the tanh activation.

Unfortunately, the canonical activation is not for all EDF distributions a desirable candidate for a VAE model. The canonical activation of the Gamma distribution (which also belongs to the EDF) is given by $-1/\eta$, with support in \mathbb{R}^+ . It is not favourable to limit the support, since this would place restrictions on the linear predictor $\eta = W \cdot Z + b$ and hence on the weights and biases. A common workaround from GLM theory is to use the activation $\exp \eta$, but this function does not produce the desired linear mapping in (3).

3.3 Approximating the ELBO

In this section, the new interpretation of the decoder as GLM allows to approximate the ELBO (see Proposition 1), by linearising the log-partition function F . We can use the results to make statements on the choice of the activation function (see Section 3.4), to derive weight and bias initializations (see Section C.3 of the supplementary material and the results in Section 4) or to monitor the training of an intractable VAE with a tractable reference point (see Section 4).

Proposition 1. *Consider N observations $x^{(1)}, \dots, x^{(N)}$ of a d -dimensional r.v. X . Assume the independent identical marginals of X given Z belong to the same EDF distribution with functions F and K as in (2). Each marginal distribution has a parameter ϑ_j ($j = 1, \dots, d$) and $\varphi > 0$ is the same. For a VAE as in Section 3, we assume the one-layer decoder has a linearly canonical activation function m , s.t. $\vartheta = \beta \cdot \eta$, where $\beta \in \mathbb{R} \setminus \{0\}$, $\eta = W \cdot Z + b$, $W \in \mathbb{R}^{d \times \kappa}$ and $b \in \mathbb{R}^d$.*

³We apply functions with one-dimensional support on vectors, which is interpreted as element wise operations.

Then, there exists an approximative representation for \mathcal{L} as in (1), around an arbitrary point $\vartheta_0 \in \Theta$, that admits an optimal solution for $\mu_z^{(i)}$ and $\Sigma_z^{(i)}$, such that it can be written as

$$\begin{aligned}\widehat{\mathcal{L}}(W, b) = & \frac{1}{N} \sum_{i=1}^N \left[-\frac{1}{2} \left(y^{(i)} - b \right)^T \left(WW^T + \frac{1}{\alpha} I_d \right)^{-1} \left(y^{(i)} - b \right) \right] \\ & - \frac{1}{2} \log \left| WW^T + \frac{1}{\alpha} I_d \right| - \frac{d}{2} \log(\alpha) + D,\end{aligned}\quad (4)$$

where $y^{(i)}$, α and D are constant in W and b .

Setting $\gamma_0 := F(\vartheta_0)$, $\gamma_1 := F'(\vartheta_0)$, $\gamma_2 := F''(\vartheta_0)$ and $\mathbb{1} = (1, \dots, 1)^T \in \mathbb{R}^d$, we have $\alpha := \frac{\beta^2 \gamma_2}{\varphi}$, $y^{(i)} := y^{(i)}(\beta, \vartheta_0) = \frac{1}{\beta \gamma_2} (x^{(i)} + (\gamma_2 \vartheta_0 - \gamma_1) \mathbb{1})$ and

$$D := D(\varphi, \vartheta_0) = -\frac{d\gamma_0}{\varphi} + \frac{\vartheta_0}{\varphi} \mathbb{1}^T \bar{x} + \frac{1}{N} \sum_{i=1}^N \widehat{K} \left(x^{(i)}, \varphi \right) + \frac{1}{2\gamma_2 \varphi} \frac{1}{N} \sum_{i=1}^N \left\| x^{(i)} - \gamma_1 \mathbb{1} \right\|_2^2,$$

where $\widehat{K} \left(x^{(i)}, \varphi \right) := \sum_{j=1}^d K(x_j^{(i)}, \varphi)$ and \bar{x} denotes the sample mean.

See Section B.2 of the supplementary material for the proof. Usually, we set $\vartheta_0 = 0$. See Table 2 in Section A of the supplementary material for different EDF distributions and linearly canonical activation functions as well as the parameters for Proposition 1 with this choice of ϑ_0 .

To derive this alternative expression, we made use of a Taylor approximation. Therefore, we can quantify the approximation error via the corresponding remainder.

Corollary 1. *Under the assumptions of Proposition 1, the error to the original ELBO in (1) is given by $\mathbb{E}_{q_\phi} \left[\sum_{j=1}^d -R_2(\vartheta_j; F, \vartheta_0) \right]$, where $R_2(\vartheta; F, \vartheta_0)$ denotes the Taylor remainder for approximating the log-partition function F at the point ϑ_0 with a 2nd degree Taylor approximation. If we assume F to originate*

- from a Gaussian distribution, then $R_2(\vartheta_j; F, \vartheta_0) = 0$ for all $\vartheta_0 \in \Theta$.

Consider $\vartheta_0 = 0$, if we assume F to originate

- from a Binomial distribution, then $0 \leq -R_2(\vartheta_j; F, 0) \leq n \frac{\vartheta_j^4}{8 \cdot 24}$.
- from a Poisson distribution, then $\frac{-\exp(\vartheta_j) \vartheta_j^3}{6} \leq -R_2(\vartheta_j; F, 0) \leq \frac{-\vartheta_j^3}{6}$.

See Section B.3 of the supplementary material for the proof. Since in our setting ϑ_j is Gaussian under q_ϕ , the moments for given parameters ϕ can be calculated straight forward.

Corollary 1 highlights how our theory generalizes the works of Dai et al. (2018), Lucas et al. (2019) and Sicks et al. (2020). Under the Gaussian assumption with linearly canonical activation, $\widehat{\mathcal{L}}$ is exact. Then, Proposition 1 yields an equivalent result as given by Dai et al. (2018) and extended by Lucas et al. (2019). For the Bernoulli distribution, the expected difference is positive. Hence, with $\widehat{\mathcal{L}}$ from Proposition 1 we approximate the ELBO in (1) from below. The result for the sigmoid activation is the same lower bound as reported in Sicks et al. (2020). Thus, the ELBO is bounded from both sides as naturally its values have to be negative and we have

$$\widehat{\mathcal{L}} \leq \mathcal{L} \leq 0. \quad (5)$$

Given the assumptions in Proposition 1, we retrieve the optimal $\mu_z^{(i)}$ and $\Sigma_z^{(i)}$ for $\widehat{\mathcal{L}}$ as a direct consequence of the proof of Proposition 1 in the following corollary.

Corollary 2. *For an observation $x^{(i)}$ of X , the optimal closed form solutions for $\mu_z^{(i)}$ and $\Sigma_z^{(i)}$ for $\widehat{\mathcal{L}}$ in Proposition 1 are given by $\hat{\Sigma}_z := \hat{\Sigma}_z^{(i)} = (I_\kappa + \alpha W^T W)^{-1}$ and $\hat{\mu}_z^{(i)} = \alpha \hat{\Sigma}_z W^T (y^{(i)} - b)$, with $y^{(i)}$ and α as in Proposition 1.*

3.4 MLE and optimal solution

In the following, we analyse the optimal values of W and b for $\hat{\mathcal{L}}$ and highlight important properties. To do so, we rewrite the objective and obtain a similar representation as in Tipping and Bishop (1999),

$$\hat{\mathcal{L}}(W, b) = D - \frac{1}{2} (d \log(\alpha) + \log |C| + \text{tr}(C^{-1}S)), \quad (6)$$

with $C := WW^T + \frac{1}{\alpha}I_d$ and $S := \frac{1}{N} \sum_{i=1}^N (y^{(i)} - b)(y^{(i)} - b)^T$. According to Tipping and Bishop (1999), the MLE for \hat{b} is given by the sample mean of $y^{(1)}, \dots, y^{(N)}$. Therefore, S with \hat{b} becomes the sample covariance (we denote it as \hat{S}). For later purposes, we also define the sample covariance matrix of $x^{(1)}, \dots, x^{(N)}$ as \hat{S}^x . With $\lambda_1, \dots, \lambda_d$ we denote the (ordered) eigenvalues of the matrix \hat{S} and the same for $\lambda_1^x, \dots, \lambda_d^x$ and \hat{S}^x . It holds $\lambda_j = \frac{\lambda_j^x}{\beta^2 \gamma_2^2}$ for $j = 1, \dots, d$, with β and γ_2 from Proposition 1. In a similar way to Tipping and Bishop (1999), we can derive the MLE of W as

$$\hat{W} = U_\kappa \left(K_\kappa - \frac{1}{\alpha} I_\kappa \right)^{1/2} R, \quad (7)$$

where $U_\kappa \in \mathbb{R}^{d \times \kappa}$ is composed of κ eigenvectors of the matrix \hat{S} . These eigenvectors are associated with the κ biggest eigenvalues $\lambda_1, \dots, \lambda_\kappa$. $K_\kappa \in \mathbb{R}^{\kappa \times \kappa}$ is a diagonal matrix with entries

$$k_j = \begin{cases} \lambda_j, & \lambda_j \geq \frac{1}{\alpha} \\ \frac{1}{\alpha}, & \text{else.} \end{cases} \quad (8)$$

$R \in \mathbb{R}^{\kappa \times \kappa}$ is an arbitrary rotation matrix, which implies that our optimal solution is invariant to rotations. Dai et al. (2018) show this as well as invariance to permutations in their Theorem 2.

It is possible to have $\text{rank}(\hat{W}) < \kappa$, and the term $\gamma_2 \varphi$ (for $\lambda_1^x, \dots, \lambda_d^x$) controls how much columns in the matrix $R^T \hat{W}$ are zero. We interpret this as a consequence of the auto-pruning property of VAE: If the data signal is not strong enough, it is pruned away.

Further, if φ exists (e.g. in the Gaussian case), the MLE for φ is given by $\hat{\varphi} = \frac{\beta^2 \gamma_2}{(d - \kappa)} \sum_{i=\kappa+1}^d \lambda_i = \frac{1}{(d - \kappa) \gamma_2} \sum_{i=\kappa+1}^d \lambda_i^x$. We interpret this as the variance lost due to the dimension reduction.

Given the MLE, the following result shows that the choice of the activation function does not matter for the maximal value of $\hat{\mathcal{L}}$ for non-degenerated cases (i.e. $\lambda_j^x \geq \gamma_2 \varphi$ for $j = 1, \dots, \kappa$). The same can be shown for the bounds in Corollary 1. It is notable that neither maximal point nor bounds depend on the choice of the activation. We also observe this in our simulations. A possible reason for this could be that we restrict the theory to linearly canonical activations.

Proposition 2. *Assume that for the first κ eigenvalues of \hat{S}^x we have $\lambda_j^x \geq \gamma_2 \varphi$ for $j = 1, \dots, \kappa$. At the optimal points \hat{W} and \hat{b} , the maximum of $\hat{\mathcal{L}}$ in Proposition 1 becomes independent of β and can be written as*

$$\hat{\mathcal{L}}(\hat{W}, \hat{b}) = D(\vartheta_0, \varphi) - \frac{1}{2} \left(\sum_{i=1}^{\kappa} \log \left(\frac{\lambda_j^x}{\gamma_2 \varphi} \right) + \kappa + \sum_{i=\kappa+1}^d \frac{\lambda_j^x}{\gamma_2 \varphi} \right). \quad (9)$$

If less than κ eigenvalues fulfil the assumption, $\hat{\mathcal{L}}(\hat{W}, \hat{b})$ depends on β and is maximal for $\beta \rightarrow \infty$.

See Section B.4 of the supplementary material for the proof.

4 Simulation results

In this section, we provide simulation results to illustrate our theoretical results from Section 3. We focus on the Bernoulli case, popular for image data. According to Corollary 1, $\hat{\mathcal{L}}$ from Proposition 1 becomes a lower bound yielding (5). Therefore, we expect the ELBO of VAE with an according architecture to lie above $\hat{\mathcal{L}}$. The essential messages of the simulations are the following:

- It is reasonable to use $\hat{\mathcal{L}}$ to analyse the training performance on real life data sets.
- The statement above is also valid for deep VAE architectures.
- The MLE points, from Section 3.4, used as initialization enhance the training performance.

For training of the nets we use the Adam optimizer by Kingma and Ba (2015) with learning rate 0.0001 and a batch size of 100. Training was done for a total of 25,000 batch evaluations. The simulations ran on a dual Intel Xeon E5-2670 with 16 CPU @ 2.6 GHz. The longest setup took about one hour of computing time.⁴

By varying the following hyper parameters, we conduct a total of 36 different simulation setups:

- Architecture: “canonical” or “deep”.
- Latent dimension κ : 2, 5 or 20.
- Last decoder activation: “sigmoid” or “tanh”.
- Data: “synthetic”, “frey” or “mnist”.

We compare our initialization scheme (“MLE-B”) to a benchmark (“Bench”) given by He et al. (2015). The initialization schemes and different hyper parameters are explained in detail in Section C of the supplementary material. Figure 1 shows the result of training the two different initialized VAE on the frey dataset with two different architectures “deep” and “canonical”. We set $\kappa = 2$ and the decoder activation as sigmoid function.

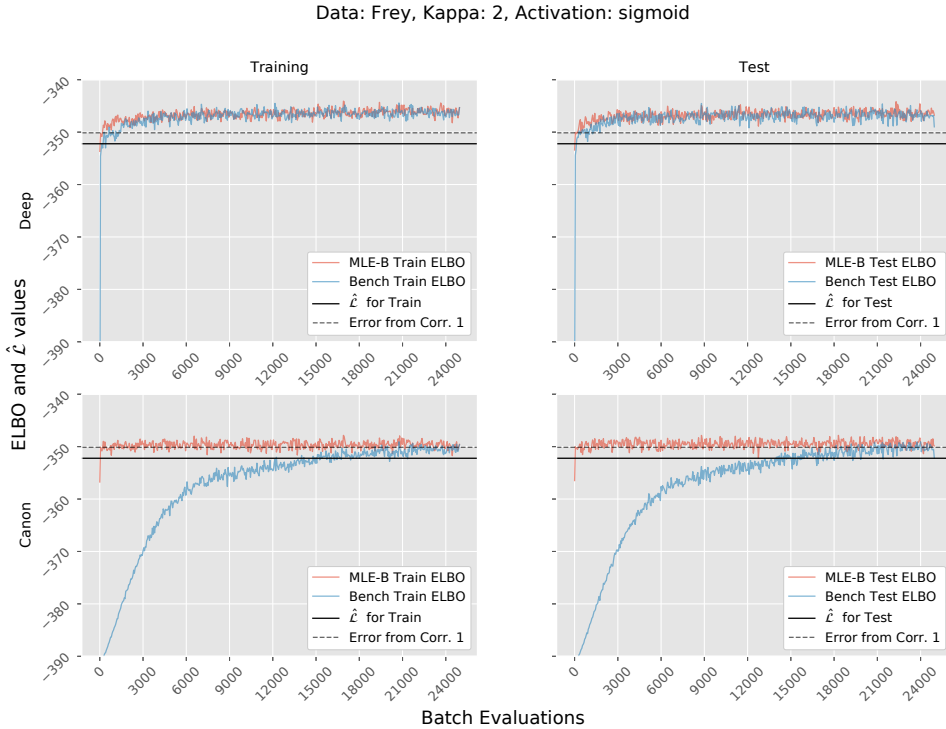


Figure 1: The picture shows two different setups deep and canonical with frey data, $\kappa = 2$ and sigmoid activation. Displayed are the ELBOs of both initialisations MLE-B and Bench as well as the lower bound $\hat{\mathcal{L}}$ and the expected error as provided by Corollary 1, calculated with MLE. On the left the values are calculated with the training data and on the right with test data.

In Figure 1, the bound $\hat{\mathcal{L}}$ is reasonable and both architectures do not perform significantly better. The results of all simulation schemes can be found in Section C.4 of the supplementary material. Comparing these simulation results and also considering Figure 1, we observe the following:

⁴Our code together with a readme file for execution can be found in the folder “vae_exp_fam_code” provided together with the supplementary materials.

- For the canonical architecture, the initialization MLE-B converges directly, whereas the Benchmark takes much more time. The end values are comparable. For the deep architecture, the performance of the two initialization methods mostly shows a small initial advantage of MLE-B which, however, is not as clear as in the canonical architecture.
- Different decoder activations yield similar results. This observation agrees with our theoretical result that the activation affects neither bound nor optimal $\hat{\mathcal{L}}$ (see Section 3.4).
- In no simulation setup a net was over-fitting, not even for large values of κ with synthetic data, where a much smaller κ was needed. This property of VAE is known as auto-pruning.
- It seems that MLE-B needs a very short burn-in period to perform according to Corollary 1. We believe that the offset at the beginning originates from not readily initialized hidden layers (see Section C.1 of the supplementary material).

5 Conclusion

We have established a new framework for VAE, by interpreting the decoder of a VAE as a GLM. Given this framework, we derive and analyse an approximation to the ELBO. We derive MLE for this approximation and provide simulation results validating the theory on real world datasets, like the frey and mnist dataset. The results here generalize previous work in this field.

Possible extensions and research directions based on our findings are:

- A deep decoder as opposed to the one-layer version here, can be considered. A possible way would be to think of the last layer of a deep decoder as GLM, as in Wüthrich (2020).
- Distributions like the Gamma distribution also belong to the EDF but are not yet covered by our theory. Future research on possible data transformations should extend our results for this. Furthermore, it is also interesting to extend the GLM approach to cover popular activations such as ReLU and variations of it.

Broader Impact

As our contributions are of theoretical nature, we do not believe that the intention of this section is applicable for this work.

References

Aitchison, J. and S. M. Shen
 1980. Logistic-normal distributions: Some properties and uses. *Biometrika*, 67(2):261–72.

Baldi, P. and K. Hornik
 1989. Neural networks and principal component analysis: Learning from examples without local minima. *Neural Networks*, 2(1):53–58.

Barndorff-Nielsen, O.
 2014. *Information and exponential families: in statistical theory*. John Wiley & Sons.

Blaschke, T., M. Olivecrona, O. Engkvist, J. Bajorath, and H. Chen
 2018. Application of Generative Autoencoder in De Novo Molecular Design. *Molecular Informatics*, 37(1-2).

Bourlard, H. and Y. Kamp
 1988. Auto-Association by Multilayer Perceptrons and Singular Value Decomposition. *Biol. Cybern.*, 59:291–294.

Dai, B., Y. Wang, J. Aston, and D. Wipf
 2018. Connections with Robust PCA and the Role of Emergent Sparsity in Variational Autoencoder Models. *Journal of Machine Learning Research*, 19:1–42.

Dai, B. and D. Wipf
 2019. Diagnosing and Enhancing VAE Models. In *7th International Conference on Learning Representations, ICLR*.

Duan, X., J. Liu, and E. Zhang
 2019. Efficient image encryption and compression based on a VAE generative model. *Journal of Real-Time Image Processing*, 16(3):765–773.

Ghosh, P., M. S. M. Sajjadi, A. Vergari, M. Black, and B. Schölkopf
 2020. From Variational to deterministic Autoencoders. In *8th International Conference on Learning Representations, ICLR*.

Goodfellow, I., Y. Bengio, and A. Courville
 2016. *Deep learning*.

He, K., X. Zhang, S. Ren, and J. Sun
 2015. Delving Deep into Rectifiers: Surpassing Human-Level Performance on ImageNet Classification. In *The IEEE International Conference on Computer Vision (ICCV)*.

Jorgensen, B.
 1986. Some Properties of Exponential Dispersion Models. *Scandinavian Journal of Statistics*, 13(3):187–197.

Jorgensen, B.
 1987. Exponential Dispersion Models. *Journal of the Royal Statistical Society. Series B (Methodological)*, 49(2):127–162.

Kingma, D. P. and J. L. Ba
 2015. Adam: A method for stochastic optimization. In *3rd International Conference on Learning Representations, ICLR*.

Kingma, D. P. and M. Welling
 2014. Auto-Encoding Variational Bayes. In *2nd International Conference on Learning Representations, ICLR*.

Kunin, D., J. M. Bloom, A. Goeva, and C. Seed
 2019. Loss Landscapes of Regularized Linear Autoencoders. In *Proceedings of the 36th International Conference on Machine Learning*.

LeCun, Y.
 2020. Keynote: The Future is Self-Supervised. In *8th International Conference on Learning Representations, ICLR*.

LeCun, Y., C. Cortes, and C. Burges
 2010. MNIST handwritten digit database. *ATT Labs [Online]*, 2.

Lee, S., J. Z. Huang, and J. Hu
 2010. Sparse Logistic Principal Components Analysis For Binary Data. *The annals of applied statistics*, 4(3):1579–1601.

Lucas, J., G. Tucker, R. Grosse, and M. Norouzi
 2019. Don't Blame the ELBO! A Linear VAE Perspective on Posterior Collapse. In *Advances in Neural Information Processing Systems 32*.

McCullagh, P. and J. Nelder
 1989. *Generalized linear models*, 2nd edition. London: Chapman and Hall.

Nair, V. and G. E. Hinton
 2010. Rectified linear units improve restricted boltzmann machines. In *Proceedings of the 27th international conference on machine learning (ICML-10)*, Pp. 807–814.

Nelder, J. A. and R. W. M. Wedderburn
 1972. Generalized Linear Models. *Source: Journal of the Royal Statistical Society. Series A (General)*, 135(3):370–384.

Sicks, R., R. Korn, and S. Schwaar
 2020. A lower bound for the ELBO of the Bernoulli Variational Autoencoder. Technical report.

Tipping, M. E. and C. M. Bishop
 1999. Probabilistic Principal Component Analysis. *Journal of the Royal Statistical Society: Series B (Statistical Methodology)*, 61(3):611–622.

van den Oord, A., O. Vinyals, and K. Kavukcuoglu
 2017. Neural Discrete Representation Learning. In *Proceedings of the 31st Conference on Neural Information Processing Systems*.

Wüthrich, M. V.
 2020. From Generalized Linear Models to Neural Networks, and Back. Technical report.

Xu, H., W. Chen, N. Zhao, Z. Li, J. Bu, Z. Li, Y. Liu, Y. Zhao, D. Pei, Y. Feng, J. Chen, Z. Wang, and H. Qiao
 2018. Unsupervised Anomaly Detection via Variational Auto-Encoder for Seasonal KPIs in Web Applications. In *World Wide Web Conference*, P. 10. ACM.

Yuan, B., X. Wang, J. Ma, C. Zhou, A. L. Bertozzi, and H. Yang
 2020. Variational Autoencoders for Highly Multivariate Spatial Point Processes Intensities. In *8th International Conference on Learning Representations, ICLR*.

Zhou, Y. and Y. Liang
 2018. Critical Points of Neural Networks: Analytical Forms and Landscape Properties. In *6th International Conference on Learning Representations, ICLR*.

A Tables and Examples

Table 1: An overview of well-known distributions that apply to our theory in Section 3.3. The functions for the representation as exponential family member as well as ϑ and φ in terms of the natural parameters are displayed.

Dist. of X	$F(\vartheta)$	$K(x, \varphi)$	ϑ	φ
$Bin(n, p)$, with n fixed	$n \log(1 + \exp(\vartheta))$	$\log \binom{n}{x}$	$\log \left(\frac{p}{1-p} \right)$	1
$Bern(p)$ $= Bin(1, p)$	$\log(1 + \exp(\vartheta))$	0	$\log \left(\frac{p}{1-p} \right)$	1
$\mathcal{N}(\mu, \sigma^2)$, with σ^2 fixed	$\frac{\vartheta^2}{2}$	$-\frac{x^2}{2\varphi} - \frac{\log(2\pi\varphi)}{2}$	μ	σ^2
$Pois(\lambda)$	$\exp(\vartheta)$	$-\log(x!)$	$\log(\lambda)$	1

Table 2: Different EDF distributions and linearly canonical activation functions as well as the parameters for the approximation in Proposition 1, with $\vartheta_0 = 0$.

Distribution of X	Activation $\mathbf{m}(z)$	β	γ_0	γ_1	γ_2
$Bin(n, p)$	$\frac{n}{1 + \exp(z)}$	1	$n \log(2)$	$n/2$	$n/4$
	$n/2 \cdot \tanh(z) + n/2$	2	$n \log(2)$	$n/2$	$n/4$
$\mathcal{N}(\mu, \lambda)$, with λ fixed	$a \cdot z$, with $a \in \mathbb{R} \setminus \{0\}$	a	0	0	1
$Pois(\lambda)$	$\exp(a \cdot z)$, with $a \in \mathbb{R} \setminus \{0\}$	a	1	1	1

Example 1 (Bernoulli distribution - sigmoid activation). *For $X \sim Bern(p(\vartheta))$, we get $F(\vartheta) = \log(1 + \exp(\vartheta))$. Hence for the canonical activation we have*

$$\mathbf{m}(\boldsymbol{\eta}) = F'(\boldsymbol{\eta}) = \frac{1}{1 + \exp(-\boldsymbol{\eta})},$$

which is the sigmoid activation.

Example 2 (Bernoulli distribution - tanh activation). *Assume $X \sim Bern(p(\vartheta))$ and set the activation as*

$$\mathbf{m}(\boldsymbol{\eta}) = 1/2 \cdot \tanh(\boldsymbol{\eta}) + 1/2.$$

As in the example before $F(\vartheta) = \log(1 + \exp(\vartheta))$ and it can be shown that

$$\vartheta = 2 \cdot \boldsymbol{\eta}.$$

B Appendix: Proofs

B.1 Auxiliary results

Lemma 2. For a d -dimensional random variable $X \sim \mathcal{N}(\boldsymbol{\mu}, \boldsymbol{\Sigma})$ it holds

$$\mathbb{E}[X^T X] = \text{tr}(\boldsymbol{\Sigma}) + \boldsymbol{\mu}^T \boldsymbol{\mu}$$

Proof. Given

$$\text{Cov}(X) = \mathbb{E}[XX^T] - \boldsymbol{\mu}\boldsymbol{\mu}^T$$

and the fact that

$$\text{tr}(\mathbb{E}[XX^T]) = \mathbb{E}[\text{tr}(XX^T)] = \mathbb{E}[X^T X]$$

yields the statement. \square

Lemma 3. Let $B, \Gamma \in \mathbb{R}^{\kappa \times \kappa}$ be symmetric positive definite matrices. Then it holds

$$B = \arg \min_{\Gamma \succ 0} \text{tr}(B\Gamma^{-1}) + \log |\Gamma|$$

and hence

$$\kappa + \log |B| = \min_{\Gamma \succ 0} \text{tr}(B\Gamma^{-1}) + \log |\Gamma|.$$

Proof. Define the two distributions $\mathcal{N}_0(\boldsymbol{\mu}, B)$ and $\mathcal{N}_1(\boldsymbol{\mu}, \Gamma)$. We have

$$\begin{aligned} & 2 \cdot D_{KL}(\mathcal{N}_0(\boldsymbol{\mu}, B) || \mathcal{N}_1(\boldsymbol{\mu}, \Gamma)) \\ &= \text{tr}(B\Gamma^{-1}) + \log |\Gamma| - \kappa - \log |B|. \end{aligned} \tag{10}$$

Now, consider that for the Kullback-Leibler-Divergence with probability distributions P and Q it holds:

- $D_{KL}(P||Q) \geq 0$ for all inputs.
- $D_{KL}(P||Q) = 0$ if and only if $P = Q$ almost everywhere.

Hence, we conclude $B = \Gamma$ in the minimum. \square

B.2 Proof of Proposition 1

Proof. To proof Proposition 1, we change the perspective. Instead of maximizing the average ELBO, we want to minimize the negative average ELBO given by

$$\begin{aligned} -\mathcal{L}(\phi, \boldsymbol{\vartheta}) := & \frac{1}{N} \sum_{i=1}^N D_{KL} \left(q_\phi(Z|x^{(i)}) || P(Z) \right) \\ & - \mathbb{E}_{Z \sim q_\phi(\cdot|x^{(i)})} \left[\log P_{\boldsymbol{\vartheta}, \varphi}(x^{(i)}|Z) \right]. \end{aligned} \tag{11}$$

Looking at (11), we see two terms. For the KL-divergence we have that

$$\begin{aligned} & 2 \cdot D_{KL} \left(q_\phi(Z|x^{(i)}) || P(Z) \right) \\ &= \text{tr}[\boldsymbol{\Sigma}_z^{(i)}] - \log |\boldsymbol{\Sigma}_z^{(i)}| + \|\boldsymbol{\mu}_z^{(i)}\|_2^2 - \kappa \end{aligned} \tag{12}$$

and for the second term (with q_ϕ as abbreviation for $q_\phi(\cdot|x^{(i)})$) we derive that

$$\begin{aligned}
& -\mathbb{E}_{q_\phi} \left[\log P_{\vartheta, \varphi}(x^{(i)}|Z) \right] \\
&= -\mathbb{E}_{q_\phi} \left[\sum_{j=1}^d \frac{x_j^{(i)} \vartheta_j(Z) - F(\vartheta_j(Z))}{\varphi} + K(x_j^{(i)}, \varphi) \right] \\
&= \frac{-1}{\varphi} \mathbb{E}_{q_\phi} \left[\sum_{j=1}^d x_j^{(i)} \vartheta_j(Z) - F(\vartheta_j(Z)) \right] - \widehat{K}(x^{(i)}, \varphi) \\
&= \frac{-1}{\varphi} \left[\mathbb{E}_{q_\phi} \left[x^{(i)T} \vartheta(Z) \right] - \mathbb{E}_{q_\phi} \sum_{j=1}^d [F(\vartheta_j(Z))] \right] - \widehat{K}(x^{(i)}, \varphi). \tag{13}
\end{aligned}$$

We see two terms, where the expectation of Z is taken into account. Using

$$\vartheta(Z) = \beta \eta(Z)$$

for the first term in (13), it follows

$$\mathbb{E}_{q_\phi} \left[x^{(i)T} \vartheta(Z) \right] = \beta x^{(i)T} (W \mu_z^{(i)} + b). \tag{14}$$

For the other term in (13) first consider that the log-partition function possesses all derivatives and is convex as stated in Lemma 1. We use a second order Taylor approximation in ϑ_0 of the log-partition function F and get

$$F(\vartheta) = T_2(\vartheta; F, \vartheta_0) + R_2.$$

Setting $\gamma_0 := F(\vartheta_0)$, $\gamma_1 := F'(\vartheta_0)$ and $\gamma_2 := F''(\vartheta_0)$ we have

$$T_2(\vartheta; F, \vartheta_0) = \gamma_0 + \gamma_1 (\vartheta - \vartheta_0) + \frac{\gamma_2}{2} (\vartheta - \vartheta_0)^2.$$

We ignore R_2 and approximate the expression, within the expectation of the second argument, in (13) and get

$$\mathbb{E}_{q_\phi} \sum_{j=1}^d [F(\vartheta_j(Z))] \approx d\gamma_0 + \mathbb{E}_{q_\phi} \left[\gamma_1 \mathbb{1}^T (\vartheta - \vartheta_0 \mathbb{1}) + \frac{\gamma_2}{2} (\vartheta - \vartheta_0 \mathbb{1})^T (\vartheta - \vartheta_0 \mathbb{1}) \right].$$

with $\mathbb{1} = (1, \dots, 1)^T \in \mathbb{R}^d$. With Lemma 2 and the fact that

$$\vartheta - \vartheta_0 \mathbb{1} \sim \mathcal{N} \left(\beta \cdot (W \mu_z^{(i)} + b) - \vartheta_0 \mathbb{1}, \beta^2 \cdot (W \Sigma_z^{(i)} W^T) \right),$$

we can rewrite this as

$$\begin{aligned}
& d(\gamma_0 - \gamma_1 \vartheta_0) + \gamma_1 \beta \mathbb{1}^T (W \mu_z^{(i)} + b) + \frac{\gamma_2 \beta^2}{2} \text{tr}(W \Sigma_z^{(i)} W^T) \\
&+ \frac{\gamma_2}{2} \left\| \beta (W \mu_z^{(i)} + b) - \vartheta_0 \mathbb{1} \right\|_2^2. \tag{15}
\end{aligned}$$

Putting the results from (14) and (15) together with (12), for our target function (11), it follows that it is approximated by

$$\begin{aligned}
-\widehat{\mathcal{L}}(\phi, W, b) &:= \frac{1}{N} \sum_{i=1}^N \left[\frac{\text{tr}[\Sigma_z^{(i)}]}{2} - \frac{\log |\Sigma_z^{(i)}|}{2} + \frac{\|\mu_z^{(i)}\|_2^2}{2} - \frac{\kappa}{2} \right. \\
&\quad - \frac{1}{\varphi} \left[\beta x^{(i)T} (W \mu_z^{(i)} + b) \right] \\
&\quad + \frac{1}{\varphi} \left[d(\gamma_0 - \gamma_1 \vartheta_0) + \gamma_1 \beta \mathbb{1}^T (W \mu_z^{(i)} + b) \right] \\
&\quad + \frac{1}{\varphi} \left[\frac{\gamma_2 \beta^2}{2} \text{tr}(W \Sigma_z^{(i)} W^T) \right] \\
&\quad + \frac{1}{\varphi} \left[\frac{\gamma_2}{2} \left\| \beta (W \mu_z^{(i)} + b) - \vartheta_0 \mathbb{1} \right\|_2^2 \right] \\
&\quad \left. - \widehat{K}(x^{(i)}, \varphi) \right].
\end{aligned}$$

All potential minima w.r.t. $\Sigma_z^{(i)}$ have to conform to

$$\hat{\Sigma}_z := \hat{\Sigma}_z^{(i)} = (I_\kappa + \alpha W^T W)^{-1}, \quad (16)$$

independent of $x^{(i)}$, with $\alpha = \frac{\gamma_2 \beta^2}{\varphi}$. Note that this expression is well-defined as per assumption, we have $\beta \neq 0$, $\varphi > 0$ and $\gamma_2 > 0$. To see that these are minima and not maxima, consider Lemma 3,

$$\kappa + \log |AA^T| = \min_{\Gamma \succ 0} \text{tr}(AA^T \Gamma^{-1}) + \log |\Gamma|,$$

where we set $\Gamma^{-1} = \Sigma_z$ and $AA^T = I_\kappa + \alpha W^T W$.

Given $\hat{\Sigma}_z$ the minimal target function evaluated at this point becomes

$$\begin{aligned} -\hat{\mathcal{L}}(\phi \setminus \{\Sigma_z\}, W, b) = & \frac{1}{N} \sum_{i=1}^N \left[\frac{\|\mu_z^{(i)}\|_2^2}{2} - \frac{1}{\varphi} \left[\beta x^{(i)T} (W \mu_z^{(i)} + b) \right] \right. \\ & + \frac{1}{\varphi} \left[d(\gamma_0 - \gamma_1 \vartheta_0) + \gamma_1 \beta \mathbf{1}^T (W \mu_z^{(i)} + b) \right] \\ & + \frac{1}{\varphi} \left[\frac{\gamma_2}{2} \left\| \beta (W \mu_z^{(i)} + b) - \vartheta_0 \mathbf{1} \right\|_2^2 \right] \\ & \left. - \hat{K}(x^{(i)}, \varphi) \right] + \frac{1}{2} \log |I_k + \alpha W^T W|. \end{aligned}$$

By rearrangement this becomes

$$\begin{aligned} -\hat{\mathcal{L}}(\phi \setminus \{\Sigma_z\}, W, b) = & \frac{1}{N} \sum_{i=1}^N \left[\frac{\|\mu_z^{(i)}\|_2^2}{2} + \frac{\beta}{\varphi} \left[(\gamma_1 \mathbf{1} - x^{(i)})^T (W \mu_z^{(i)} + b) \right] \right. \\ & + \frac{1}{\varphi} \left[\frac{\gamma_2}{2} \left\| \beta (W \mu_z^{(i)} + b) - \vartheta_0 \mathbf{1} \right\|_2^2 \right] \\ & + \frac{d}{\varphi} (\gamma_0 - \gamma_1 \vartheta_0) + \frac{1}{2} \log |I_k + \alpha W^T W| \\ & \left. - \frac{1}{N} \sum_{i=1}^N \hat{K}(x^{(i)}, \varphi) \right], \end{aligned}$$

where \bar{x} denotes the element wise sample mean. For $\mu_z^{(i)}$, we get as minimal points

$$\begin{aligned} \hat{\mu}_z^{(i)} &= \frac{\beta}{\varphi} \hat{\Sigma}_z W^T \left(x^{(i)} + (\gamma_2 \vartheta_0 - \gamma_1) \mathbf{1} - \gamma_2 \beta b \right) \\ &= \alpha \hat{\Sigma}_z W^T \left(y^{(i)} - b \right), \end{aligned} \quad (17)$$

with $y^{(i)} := y^{(i)}(\beta, \vartheta_0) = \frac{1}{\beta \gamma_2} (x^{(i)} + (\gamma_2 \vartheta_0 - \gamma_1) \mathbf{1})$. This is well-defined, since $\gamma_2 = F''(\vartheta_0) > 0$ and $\beta \neq 0$. The candidates for an optimal $\hat{\mu}_z^{(i)}$ are minima since the second derivative is a positive constant times $\hat{\Sigma}^{-1}$, which is positive definite. Given the optimal $\mu_z^{(i)}$ and $\Sigma_z^{(i)}$ our target function is only dependent on the parameters W and b . We get

$$\begin{aligned} -\hat{\mathcal{L}}(W, b) = & \frac{1}{N} \sum_{i=1}^N \left[\alpha^2 \left(y^{(i)} - b \right)^T E \left(y^{(i)} - b \right) - \alpha y^{(i)T} b + \frac{\alpha}{2} \|b\|_2^2 \right] \\ & + \frac{1}{2} \log |I_k + \alpha W^T W| \\ & + \frac{-\gamma_2 d \vartheta_0^2}{2 \varphi} + \frac{d}{\varphi} (\gamma_0 - \gamma_1 \vartheta_0) - \frac{1}{N} \sum_{i=1}^N \hat{K}(x^{(i)}, \varphi), \end{aligned} \quad (18)$$

where $E := W \left[\frac{1}{2} \hat{\Sigma}_z^2 - \hat{\Sigma}_z + \frac{\alpha}{2} \hat{\Sigma}_z W^T W \hat{\Sigma}_z \right] W^T$.

Consider the Singular Value Decomposition of $W = U \tilde{D} V^T$ with $U \in \mathbb{R}^{d \times d}$ and $V \in \mathbb{R}^{\kappa \times \kappa}$ are unitary matrices and

$$\tilde{D} = \begin{bmatrix} \delta_1 & \dots & 0 \\ \vdots & \ddots & \vdots \\ 0 & \dots & \delta_\kappa \\ \vdots & \ddots & \vdots \\ 0 & \dots & 0 \end{bmatrix} \in \mathbb{R}^{d \times \kappa}.$$

We have

$$\tilde{D}^T \tilde{D} = \begin{bmatrix} \delta_1^2 & \dots & 0 \\ \vdots & \ddots & \vdots \\ 0 & \dots & \delta_\kappa^2 \end{bmatrix}$$

and can write

$$\begin{aligned} \hat{\Sigma}_z &= \left(V(I_\kappa + \alpha \tilde{D}^T \tilde{D}) V^T \right)^{-1} \\ &= V \hat{D} V^T, \end{aligned}$$

with $\hat{D} := \text{diag} \left(\frac{1}{1 + \alpha \delta_1^2}, \dots, \frac{1}{1 + \alpha \delta_\kappa^2} \right)$. For E it follows that

$$\begin{aligned} &W \left[\frac{1}{2} \hat{\Sigma}_z^2 - \hat{\Sigma}_z + \frac{\alpha}{2} \hat{\Sigma}_z W^T W \hat{\Sigma}_z \right] W^T \\ &= W \left[V \left[\frac{1}{2} \hat{D}^2 - \hat{D} + \frac{\alpha}{2} \hat{D} \tilde{D}^T \tilde{D} \hat{D} \right] V^T \right] W^T \\ &= W \left(V \check{D} V^T \right) W^T, \end{aligned} \tag{19}$$

where we denote $\check{D} = \text{diag} \left(\frac{-1}{2(1 + \alpha \delta_1^2)}, \dots, \frac{-1}{2(1 + \alpha \delta_\kappa^2)} \right)$. The justification of the last equation becomes apparent, when we consider one respective diagonal element δ_\cdot of the diagonal matrices in the equation. We have

$$\begin{aligned} &\frac{1}{2} \frac{1}{(1 + \alpha \delta_\cdot^2)^2} - \frac{1}{1 + \alpha \delta_\cdot^2} + \frac{\alpha}{2} \frac{\delta_\cdot^2}{(1 + \alpha \delta_\cdot^2)^2} \\ &= \frac{1 - 2(1 + \alpha \delta_\cdot^2) + \alpha \delta_\cdot^2}{2(1 + \alpha \delta_\cdot^2)^2} \\ &= \frac{-1}{2(1 + \alpha \delta_\cdot^2)}. \end{aligned}$$

We can further rewrite (19) as

$$\begin{aligned} W \left(V \check{D} V^T \right) W^T &= U \tilde{D} \check{D} \tilde{D}^T U^T \\ &=: -U D U^T, \end{aligned}$$

where we have introduced

$$D := \begin{bmatrix} \text{diag} \left(\frac{\delta_1^2}{2(1 + \alpha \delta_1^2)}, \dots, \frac{\delta_\kappa^2}{2(1 + \alpha \delta_\kappa^2)} \right) & \mathbf{0} \\ \mathbf{0} & \mathbf{0} \end{bmatrix} \in \mathbb{R}^{d \times d}.$$

So for the first line in (18) of our target function, we get

$$\frac{1}{N} \sum_{i=1}^N \left[-\alpha^2 \left(y^{(i)} - b \right)^T U D U^T \left(y^{(i)} - b \right) - \alpha y^{(i)T} b + \frac{\alpha}{2} \|b\|_2^2 \right]$$

By adding and subtracting the constant term $\frac{1}{N} \sum_{i=1}^N \frac{\alpha}{2} \|y^{(i)}\|_2^2$ and concluding

$$\frac{\alpha}{2} \|y^{(i)}\|_2^2 - \alpha y^{(i)T} b + \frac{\alpha}{2} \|b\|_2^2 = \frac{\alpha}{2} \|y^{(i)} - b\|_2^2,$$

we get

$$\frac{1}{N} \sum_{i=1}^N \left[(y^{(i)} - b)^T U \left(\frac{\alpha}{2} I - \alpha^2 D \right) U^T (y^{(i)} - b) - \frac{\alpha}{2} \|y^{(i)}\|_2^2 \right].$$

We can further rewrite

$$U \left(\frac{\alpha}{2} I - \alpha^2 D \right) U^T = \frac{1}{2} \left(\frac{1}{\alpha} I_d + WW^T \right)^{-1}$$

and together with

$$\frac{1}{2} \log |I_d + \alpha W^T W| = \frac{1}{2} \log \left| \frac{1}{\alpha} I_d + WW^T \right| + \frac{d}{2} \log(\alpha)$$

we get for our target function

$$\begin{aligned} -\hat{\mathcal{L}}(W, b) &= \frac{1}{N} \sum_{i=1}^N \left[(y^{(i)} - b)^T \frac{1}{2} \left(\frac{1}{\alpha} I_d + WW^T \right)^{-1} (y^{(i)} - b) \right] \\ &\quad + \frac{1}{2} \log \left| \frac{1}{\alpha} I_d + WW^T \right| - D, \end{aligned}$$

with

$$\begin{aligned} D &:= -\frac{d}{2} \log(\alpha) - \frac{-\vartheta_0^2 \gamma_2 d}{2\varphi} - \frac{d}{\varphi} (\gamma_0 - \gamma_1 \vartheta_0) \\ &\quad + \frac{1}{N} \sum_{i=1}^N \left[\frac{\alpha}{2} \|y^{(i)}\|_2^2 + \hat{K}(x^{(i)}, \varphi) \right] \\ &= -\frac{d}{2} \log(\alpha) - \frac{d\gamma_0}{\varphi} + \frac{\vartheta_0}{\varphi} \mathbf{1}^T \bar{x} + \frac{1}{N} \sum_{i=1}^N \hat{K}(x^{(i)}, \varphi) \\ &\quad + \frac{1}{2\gamma_2 \varphi} \frac{1}{N} \sum_{i=1}^N \|x^{(i)} - \gamma_1 \mathbf{1}\|_2^2. \end{aligned}$$

□

B.3 Proof of Corollary 1

Proof. We look at the Gaussian, Binomial and Poisson cases separately and always regard one respective $\vartheta \in \Theta$.

- Gaussian case: Remember that we have $F(\vartheta) = \frac{\vartheta^2}{2}$. For any $\vartheta_0 \in \Theta$ it follows directly that all third or higher derivatives of F are zero and we are done.
- Binomial case: First, we realize that the third derivative of $F(\vartheta) = n \log(1 + \exp(\vartheta))$ at $\vartheta_0 = 0$ is equal to zero. We can conclude that in 0 a second order Taylor approximation is the same as a third order approximation and the Remainder is given in the Lagrange form by

$$R_2(\vartheta; F, 0) = R_3(\vartheta; F, 0) = \frac{F^{(4)}(\xi)}{4!} \vartheta^4,$$

with ξ in between ϑ and ϑ_0 . The fourth derivative, given by

$$F(\vartheta)^{(4)} = n \frac{e^\vartheta (-4e^\vartheta + e^{2\vartheta} + 1)}{(e^\vartheta + 1)^4},$$

has it's image in $[-n/8, n/24]$. Therefore, we can bound $R_2(\vartheta; F, 0)$ from below with

$$R_2(\vartheta; F, 0) \geq n \frac{-\vartheta^4}{8 \cdot 4!}.$$

To bound the remainder from above, notice that

$$F(\vartheta)^{(3)} = -n \frac{e^\vartheta (e^\vartheta - 1)}{(e^\vartheta + 1)^3}$$

is point symmetric to zero, with negative values if $\vartheta > 0$ and positive values if $\vartheta < 0$. We can write

$$R_2(\vartheta; F, 0) = \frac{F^{(3)}(\xi)}{3!} \vartheta^3 = \frac{-|F^{(3)}(\xi)|}{3!} |\vartheta|^3 \leq 0.$$

This yields the statement. \square

- Poisson case: We have $F(\vartheta) = \exp(\vartheta)$ and can write the remainder in Lagrange form as

$$R_2(\vartheta; F, 0) = \frac{\exp(\xi)}{6} \vartheta^3,$$

with ξ in between ϑ and 0. Consider the two cases $\vartheta < 0$ and $\vartheta \geq 0$. For the case $\vartheta < 0$ we have

$$0 \geq R_2(\vartheta; F, 0) = \frac{\exp(\xi)}{6} (-|\vartheta|^3) \geq \frac{-|\vartheta|^3}{6} = \frac{\vartheta^3}{6}.$$

For the case $\vartheta \geq 0$ we have

$$\frac{\exp(\vartheta)}{6} \vartheta^3 \geq R_2(\vartheta; F, 0) \geq \frac{\vartheta^3}{6}.$$

Combining those two cases yields the statement. \square

B.4 Proof of Proposition 2

Proof. First we look at C as defined in Section 3.4. For the optimal point \hat{W} as in (7) we define

$$\begin{aligned} \hat{C} &:= \hat{W} \hat{W}^T + \frac{1}{\alpha} I_d \\ &= U \begin{bmatrix} K_\kappa & \mathbf{0} \\ \mathbf{0} & 1/\alpha I_{d-\kappa} \end{bmatrix} U^T, \end{aligned}$$

where $U \in \mathbb{R}^{d \times d}$ is the orthonormal matrix from the SVD of the sample covariance $\hat{S} = U \Lambda U^T$. Therefore, we have

$$\log |\hat{C}| = \sum_{i=1}^{\kappa} \log(k_i) - (d - \kappa) \cdot \log(\alpha)$$

and

$$\begin{aligned} \text{tr}(\hat{C}^{-1} \hat{S}) &= \text{tr} \left(U \begin{bmatrix} K_\kappa & \mathbf{0} \\ \mathbf{0} & 1/\alpha I_{d-\kappa} \end{bmatrix}^{-1} U^T U \Lambda U^T \right) \\ &= \sum_{i=1}^{\kappa} \frac{1}{k_i} \cdot \lambda_i + \sum_{i=\kappa+1}^d \alpha \lambda_i. \end{aligned}$$

Inserting this into $\hat{\mathcal{L}}$ from (6) yields

$$\hat{\mathcal{L}}(\hat{W}, \hat{b}) = D - \frac{1}{2} \left(\kappa \log(\alpha) + \sum_{i=1}^{\kappa} \log(k_i) + \sum_{i=1}^{\kappa} \frac{1}{k_i} \cdot \lambda_i + \sum_{i=\kappa+1}^d \alpha \lambda_i \right)$$

Note,

$$\lambda_j = \frac{\lambda_j^x}{\beta^2 \gamma_2^2} \quad \text{for } j = 1, \dots, d,$$

for the eigenvalues of the covariance matrix \hat{S}^x and

$$\alpha \cdot k_j = \begin{cases} \alpha \cdot \lambda_j, & \alpha \cdot \lambda_j \geq 1 \\ 1, & \text{else} \end{cases} = \begin{cases} \frac{\lambda_j^x}{\gamma_2 \varphi}, & \lambda_j^x \geq \gamma_2 \varphi \\ 1, & \text{else.} \end{cases} \quad (20)$$

Let's first assume that for the first κ eigenvalues we have $\lambda_j^x \geq \gamma_2 \varphi$ for $j = 1, \dots, \kappa$.

Then, we get

$$\hat{\mathcal{L}}(\hat{W}, \hat{b}) = D - \frac{1}{2} \left(\sum_{i=1}^{\kappa} \log \left(\frac{\lambda_j^x}{\gamma_2 \varphi} \right) + \kappa + \sum_{i=\kappa+1}^d \frac{\lambda_j^x}{\gamma_2 \varphi} \right)$$

and are done. Now, let us assume that at least for the $1 < n \leq \kappa$ lowest eigenvalues it holds $\lambda_j^x < \gamma_2 \varphi$. We get

$$\hat{\mathcal{L}}(\hat{W}, \hat{b}) = D - \frac{1}{2} \left(\sum_{i=1}^{\kappa-n} \log \left(\frac{\lambda_j^x}{\gamma_2 \varphi} \right) + (\kappa - n) + \sum_{i=n}^{\kappa} \frac{\lambda_j^x}{\beta^2 \gamma_2^2} + \sum_{i=\kappa+1}^d \frac{\lambda_j^x}{\gamma_2 \varphi} \right).$$

□

C Simulation

C.1 Architecture, latent dimension κ and the last decoder activation

For the architecture, we look at two different versions, which we denote as “deep” and “canonical”. The deep architecture is given as in Dai et al. (2018), by

$$x(d) \rightarrow E_1(2000) \rightarrow E_2(1000) \rightarrow \mu_z(\kappa) \rightarrow D_1(1000) \rightarrow D_2(2000) \rightarrow \hat{x}(d), \\ \searrow \log \sigma_z^2(\kappa) \nearrow$$

where E/D denote encoder/decoder layers and the values in the brackets indicate the dimension of the layer. So, κ is the dimension of the latent space and we use the values 2, 5 and 20 for different simulation setups.

The canonical architecture is given by

$$x(d) \rightarrow E_1(2000) \rightarrow E_2(d) \rightarrow \mu_z(\kappa) \rightarrow \hat{x}(d). \\ \searrow \log \sigma_z^2(\kappa) \nearrow$$

The canonical architecture conforms to the assumptions of Proposition 1.

The hidden layers of the encoder and the decoder are implemented with ReLU-activation (see Nair and Hinton 2010), which is known to be highly expressive. The “ μ_z ”- and “ $\log \sigma_z^2$ ”- layer have linear activations. The last layer “ \hat{x} ” has either as sigmoid or a tanh as activation as reported in Table 2.

Apart from the fact that we expect both architectures to provide a better loss than provided by our theoretical bound, it should also be able to represent the optimal $\hat{\mu}_z^{(i)}$ and diagonal entries of the optimal $\hat{\Sigma}_z^{(i)}$ from Corollary 2, if necessary.

C.2 Data

We consider three datasets: a synthetic data set (we describe the construction at the end of this chapter), the mnist dataset (see LeCun et al. 2010) and the frey dataset.⁵ Each set is transformed to only have values in between 0 and 1. As training/test split, we have

- synthetic: 6700 / 3300

⁵Taken from <https://cs.nyu.edu/~roweis/data.html>

- mnist: 60000 / 10000
- frey: 1316 / 649

The synthetic data is constructed in the fashion of Lee et al. (2010). For $k = 2$, $N = 10000$ and $d = 200$, we generate two matrices $A \in \mathbb{R}^{N \times k}$ and $B \in \mathbb{R}^{d \times k}$. A is identifiable with principal components and B with (sparse) loading vectors of a PCA. The two-dimensional principal components $a^{(i)}(i = 1, \dots, N)$ of A are drawn from normal distributions, so that $a_1^{(i)} \sim \mathcal{N}(0, 0.09)$ and $a_2^{(i)} \sim \mathcal{N}(0, 0.25)$. The sparse loading vectors are constructed by setting B to zero except for $b_{j,1} = 1, j = 1, \dots, 20$ and $b_{j,2} = 1, j = 21, \dots, 40$.

Given A and B we calculate

$$\Xi := A \cdot B^T$$

and the probability matrix Π , with

$$\Pi = \sigma(\Xi),$$

where we apply the sigmoid function $\sigma(\cdot)$ element-wise. We then use the probabilities $\Pi_j^{(i)}$ to independently draw samples

$$x_j^{(i)} \sim \text{Bern}(\Pi_j^{(i)}).$$

With the data $X_{Data} := (x_j^{(i)})_{i=1, \dots, N; j=1, \dots, d}$, we conduct the simulation.

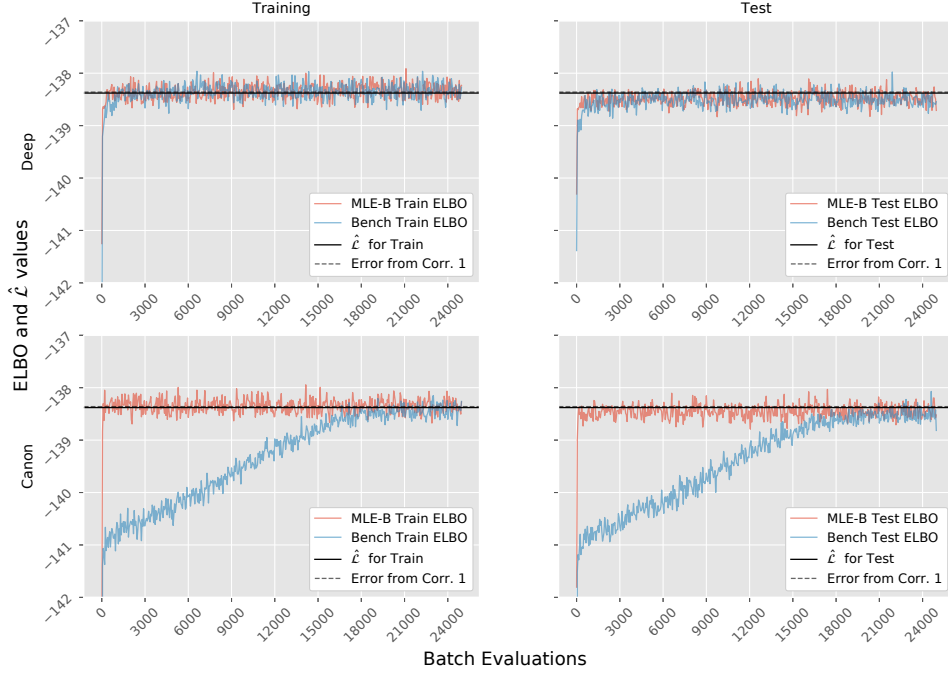
C.3 Initialization

In each simulation, we compare two competing VAE with the same architecture and different initialization. We call these initializations “Bench” (benchmark) and “MLE-B” (MLE - based). For the benchmark, all network weights and biases are initialized as proposed by He et al. (2015). This initialization particularly considers rectifier non-linearities. For MLE-B we use the same initialization except for the weights and biases of the “ μ_z ”, “ $\log \sigma_z^2$ ”- and “ \hat{x} ”-layer. We initialize these layers according to Corollary 2 and the MLE from Section 3.4. These values are always calculated only on basis of the training data.

In case of over-parametrized nets, more edges lead into the affected layers than we need for MLE-B. This problem only concerns the weights and not the biases. We solve this by initializing not needed dimensions of the weights with zero.

C.4 Simulation results

Data: Synthetic, $\kappa = 2$, Activation: sigmoid



Data: Synthetic, $\kappa = 2$, Activation: tanh

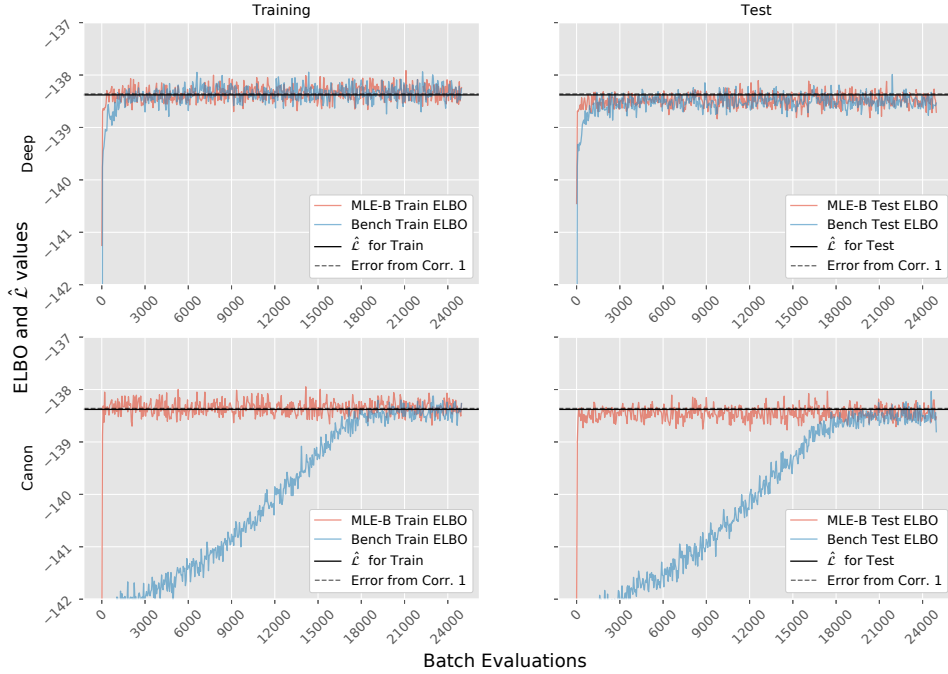


Figure 2: The pictures show the setups deep and canonical with synthetic data, $\kappa = 2$ and sigmoid activation on top and tanh on bottom. Displayed are the ELBOs of both initialisations MLE-B and Bench as well as the lower bound \hat{L} and the expected error as provided by Corollary 1, calculated with MLE. On the left the values are calculated with the training data and on the right with test data.

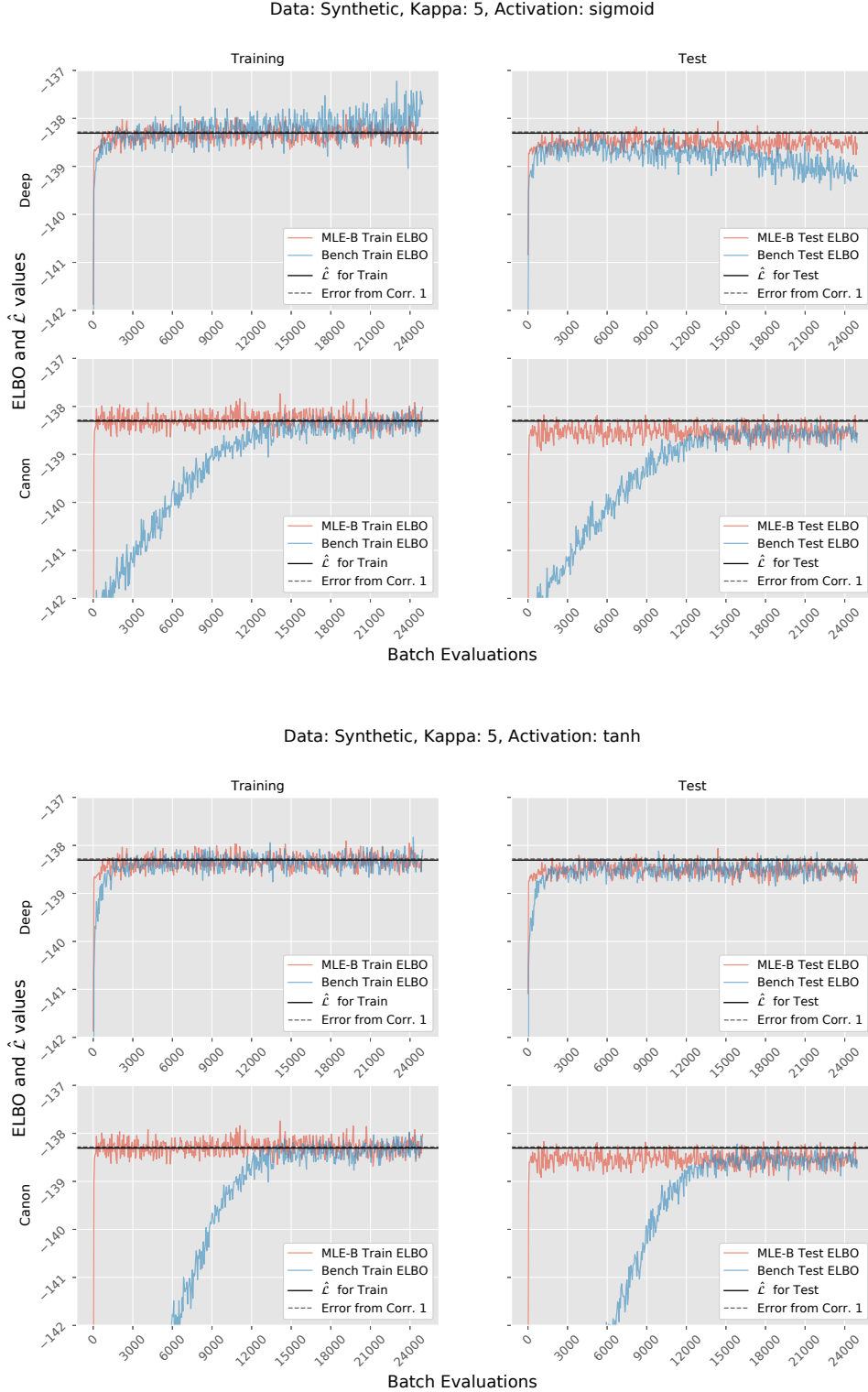


Figure 3: The pictures show the setups deep and canonical with synthetic data, $\kappa = 5$ and sigmoid activation on top and tanh on bottom. Displayed are the ELBOs of both initialisations MLE-B and Bench as well as the lower bound $\hat{\mathcal{L}}$ and the expected error as provided by Corollary 1, calculated with MLE. On the left the values are calculated with the training data and on the right with test data.

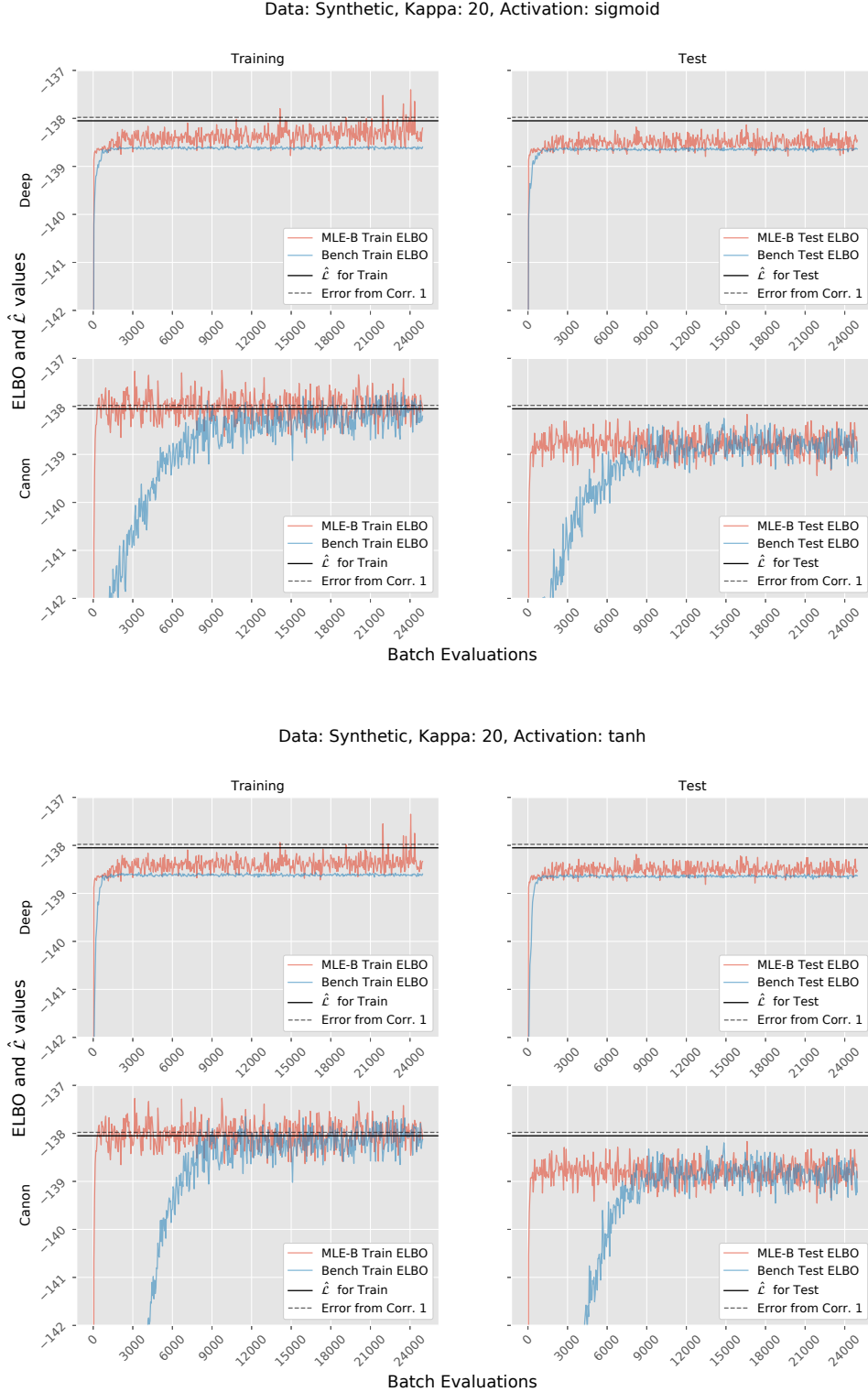


Figure 4: The pictures show the setups deep and canonical with synthetic data, $\kappa = 20$ and sigmoid activation on top and tanh on bottom. Displayed are the ELBOs of both initialisations MLE-B and Bench as well as the lower bound \hat{L} and the expected error as provided by Corollary 1, calculated with MLE. On the left the values are calculated with the training data and on the right with test data.

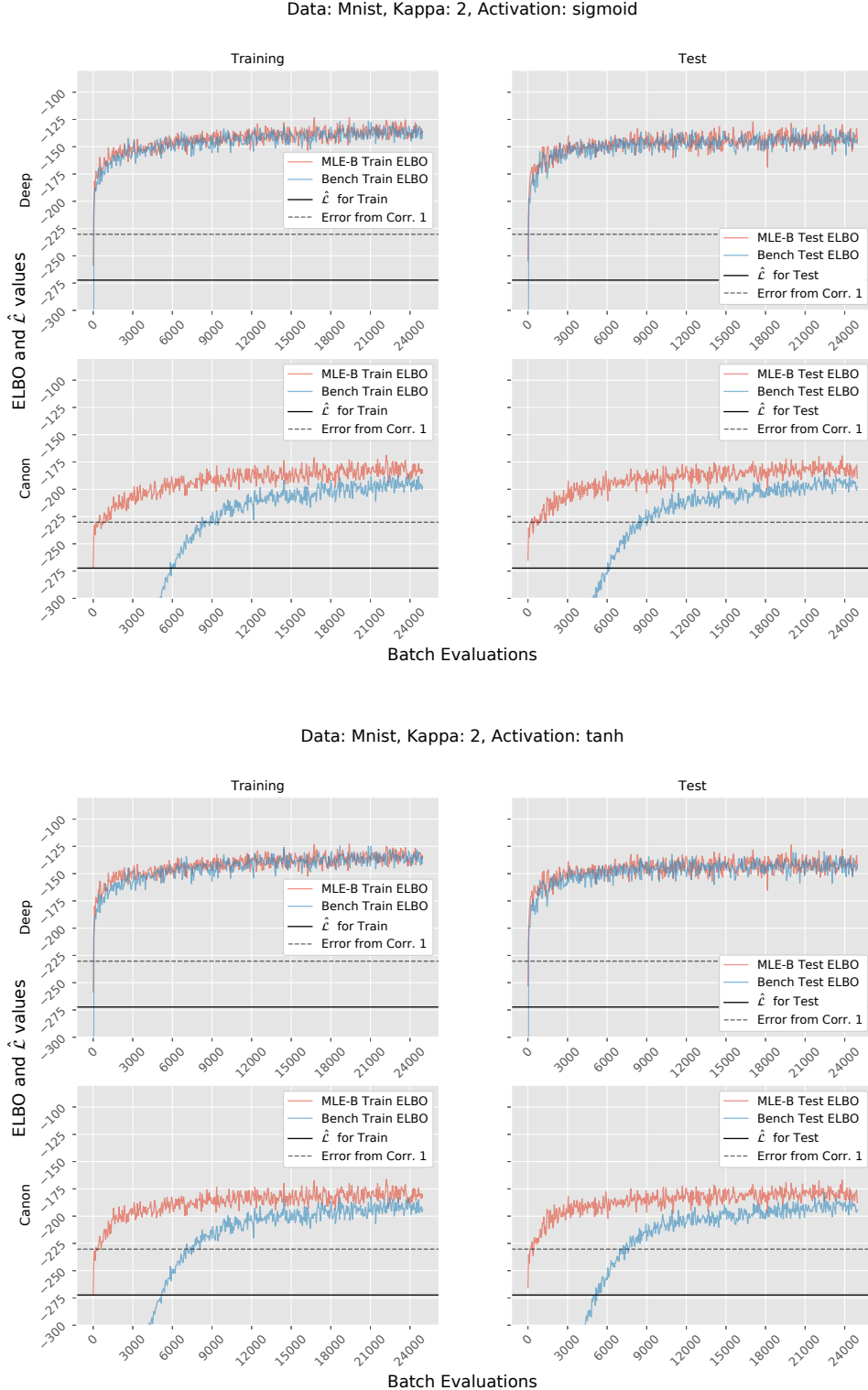


Figure 5: The pictures show the setups deep and canonical with mnist data, $\kappa = 2$ and sigmoid activation on top and tanh on bottom. Displayed are the ELBOs of both initialisations MLE-B and Bench as well as the lower bound \hat{L} and the expected error as provided by Corollary 1, calculated with MLE. On the left the values are calculated with the training data and on the right with test data.

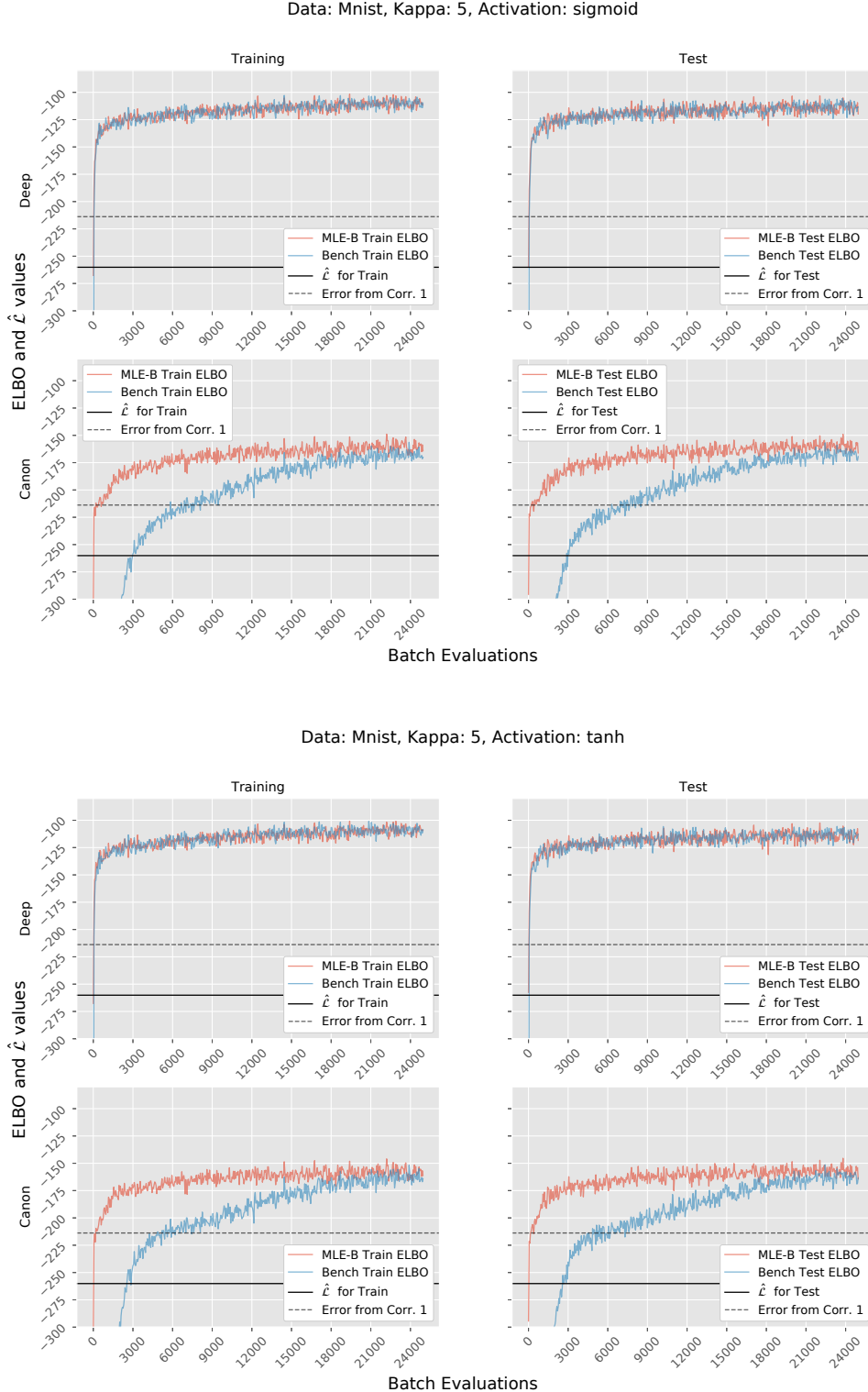


Figure 6: The pictures show the setups deep and canonical with mnist data, $\kappa = 5$ and sigmoid activation on top and tanh on bottom. Displayed are the ELBOs of both initialisations MLE-B and Bench as well as the lower bound $\hat{\mathcal{L}}$ and the expected error as provided by Corollary 1, calculated with MLE. On the left the values are calculated with the training data and on the right with test data.

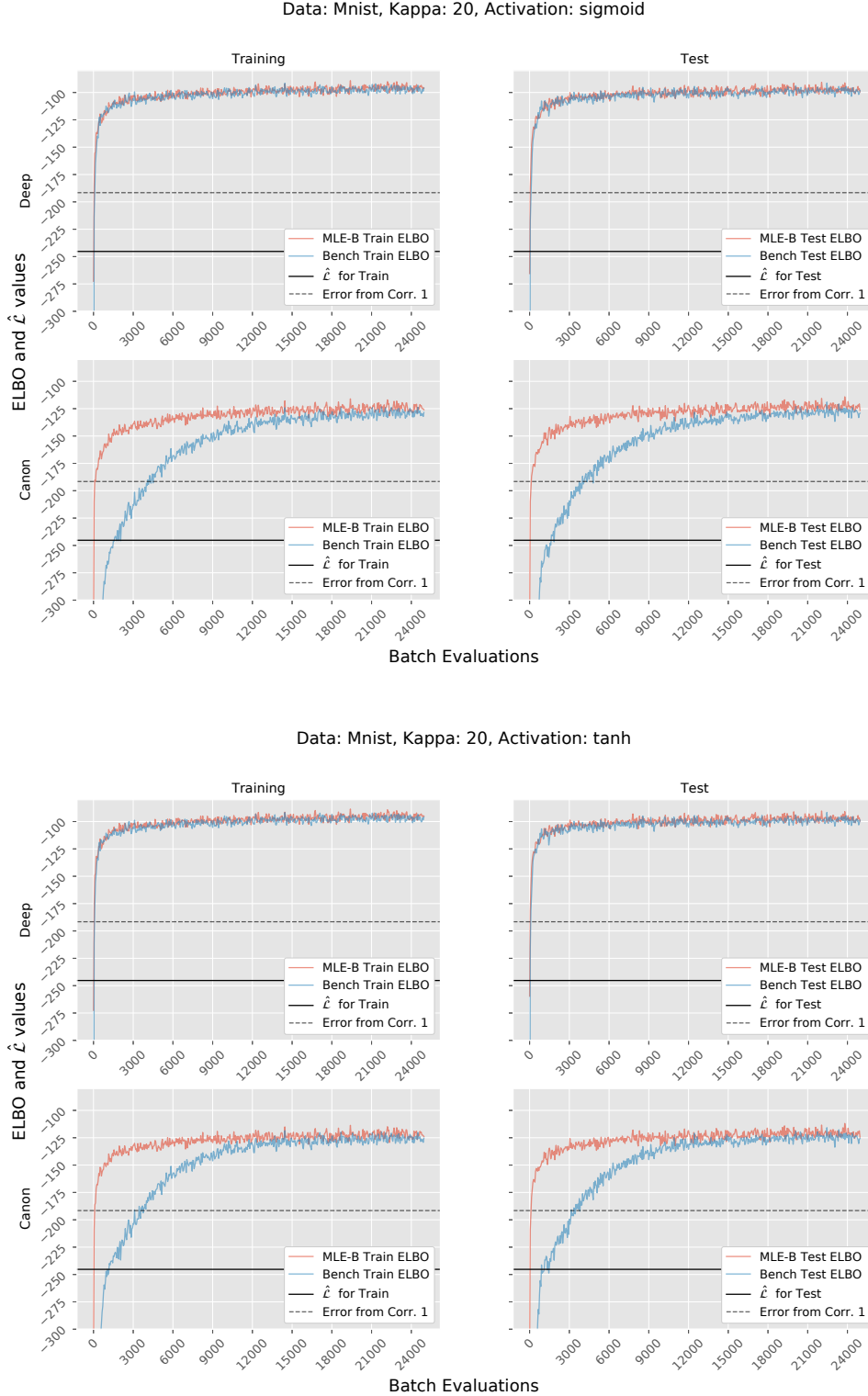


Figure 7: The pictures show the setups deep and canonical with mnist data, $\kappa = 20$ and sigmoid activation on top and tanh on bottom. Displayed are the ELBOs of both initialisations MLE-B and Bench as well as the lower bound $\hat{\mathcal{L}}$ and the expected error as provided by Corollary 1, calculated with MLE. On the left the values are calculated with the training data and on the right with test data.

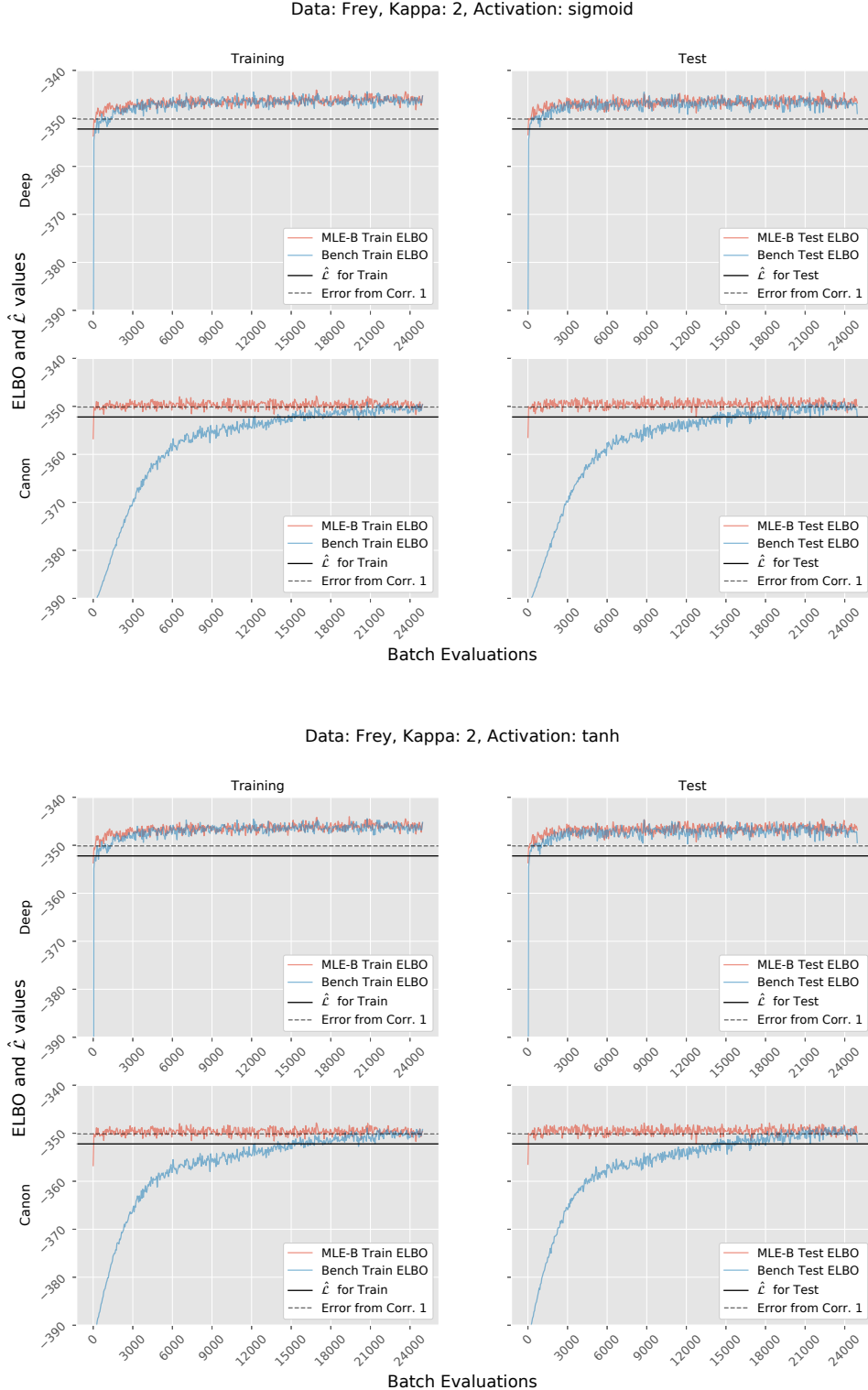


Figure 8: The pictures show the setups deep and canonical with frey data, $\kappa = 2$ and sigmoid activation on top and tanh on bottom. Displayed are the ELBOs of both initialisations MLE-B and Bench as well as the lower bound \hat{L} and the expected error as provided by Corollary 1, calculated with MLE. On the left the values are calculated with the training data and on the right with test data.

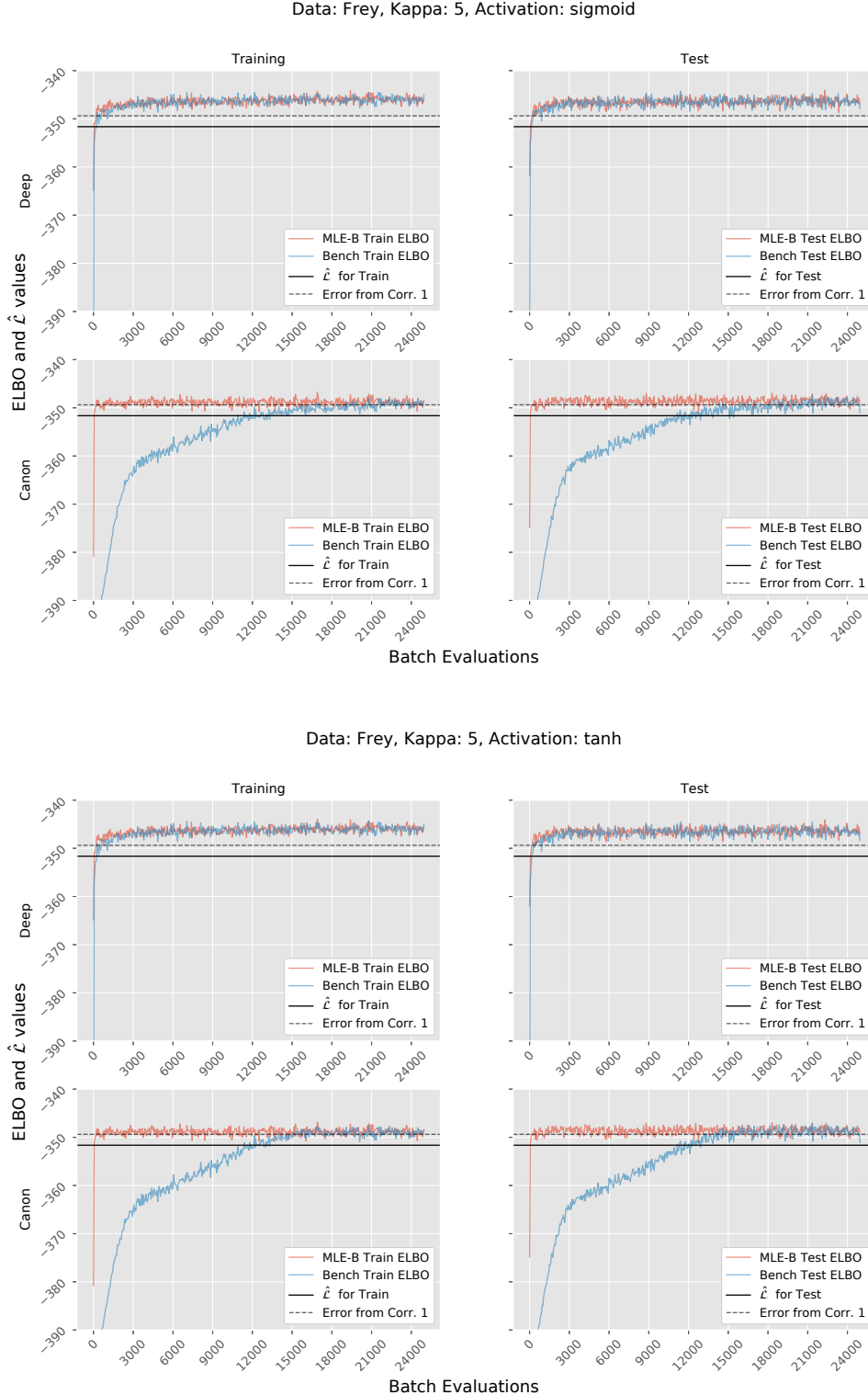


Figure 9: The pictures show the setups deep and canonical with frey data, $\kappa = 5$ and sigmoid activation on top and tanh on bottom. Displayed are the ELBOs of both initialisations MLE-B and Bench as well as the lower bound \hat{L} and the expected error as provided by Corollary 1, calculated with MLE. On the left the values are calculated with the training data and on the right with test data.

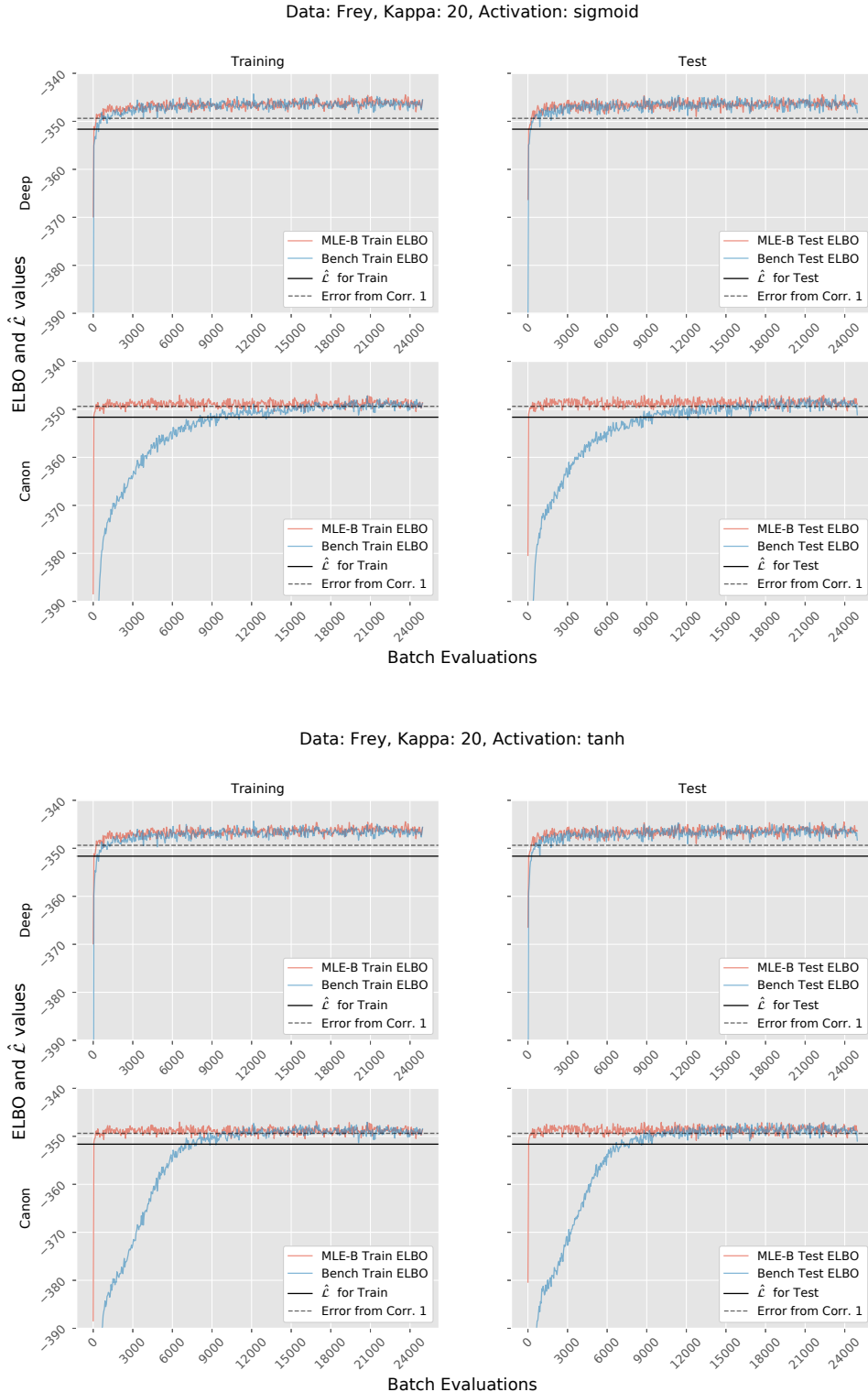


Figure 10: The pictures show the setups deep and canonical with frey data, $\kappa = 20$ and sigmoid activation on top and tanh on bottom. Displayed are the ELBOs of both initialisations MLE-B and Bench as well as the lower bound $\hat{\mathcal{L}}$ and the expected error as provided by Corollary 1, calculated with MLE. On the left the values are calculated with the training data and on the right with test data.